REVIEW

Quantum simulations with cold trapped ions

Michael Johanning, Andrés F Varón and Christof Wunderlich

Fachbereich Physik, Universität Siegen, 57068 Siegen, Germany

E-mail: wunderlich@physik.uni-siegen.de

Abstract
The control of internal and motional quantum degrees of freedom of laser-cooled trapped ions has been subject to intense theoretical and experimental research for about three decades. In the realm of quantum information science, the ability to deterministically prepare and measure quantum states of trapped ions is unprecedented. This expertise may be employed to investigate physical models conceived to describe systems that are not directly accessible for experimental investigations. Here, we give an overview of current theoretical proposals and experiments for such quantum simulations with trapped ions. This includes various spin models (e.g. the quantum transverse Ising model or a neural network), the Bose–Hubbard Hamiltonian, the Frenkel–Kontorova model, and quantum fields and relativistic effects.

(Some figures in this article are in colour only in the electronic version)

1. Introduction

Atomic ions confined in an electrodynamic trap provide us with individual quantum systems whose internal and external degrees of freedom can be controlled to a considerable degree by the experimenter. A strong motivation for early experiments with individual trapped ions arose from their potential use as frequency standards (e.g. Dehmelt (1981) and references therein). Today, by using trapped ions as frequency standards unsurpassed accuracy and precision have been reached (e.g. Rosenband *et al* (2008) and references therein), and in addition, trapped ions are used for a wide range of investigations into fundamental questions of physics, for instance in the field of quantum information science. This special issue gives an account of the many facets of research with trapped ions.

Controlling motional and internal states of trapped ions by letting them interact with electromagnetic fields, ranging from uv light to rf radiation, has led to the realization of experiments that previously (reaching well into the second half of the twentieth century) were only conceivable, by most physicists, as Gedankenexperiments. A small (and unsystematic) sample from such fascinating experiments includes the trapping and visualization of a single ion (Neuhauser *et al* 1980), the laser

cooling of a single ion to its motional ground state (Diedrich *et al* 1989), the deterministic generation and analysis of Schrödinger cat and other entangled states of massive particles, (Monroe *et al* 1996a, Leibfried *et al* 2005, Häffner *et al* 2005, Blatt and Wineland 2008) or the teleportation of ions (Riebe *et al* 2004, Barrett *et al* 2004).

While building a universal quantum computer still poses formidable experimental challenges, in particular because of the low error thresholds required for fault-tolerant computing, it appears that useful quantum simulations are more amenable to experimental efforts.

There are two common usages of the term 'quantum simulation': (i) the simulation of static and dynamic properties of quantum systems (e.g. atoms, molecules, condensed matter systems) using *classical* computers and (ii) the simulation of the properties of one quantum system by means of controlling and observing another quantum system. Here, we are concerned with the second type of research.

The purpose of a quantum simulation is to use a well-understood physical A system to simulate the static properties and the dynamics of another system B that is difficult or, for all practical purposes, even impossible to investigate experimentally (Feynman 1982, 1986, Jane *et al* 2003). In order to be able to simulate B by observing A, both

physical systems need to be described by the same underlying mathematical model.

In this paper, we give an overview of concrete proposals for performing experimental quantum simulations with laser-cooled trapped ions and of experimental work immediately relevant for using trapped ions as a quantum simulator.

2. Spin models

Interacting spins play an important role in many physical models in a variety of research fields of physics, for instance in models that are employed to describe phenomena in condensed matter physics (e.g. Schollwöck *et al* (2004) and references therein). Also, in recent years the connection between entanglement on the one hand and static and dynamic properties of many-body systems on the other hand, for instance, near quantum phase transitions (QPTs) has attracted much interest (e.g. Osterloh *et al* (2002), Amico *et al* (2008), Plenio and Virmani (2007) and references therein).

Probably the simplest approach to modelling interacting spins is the classical Ising model (Lenz 1920, Ising 1925) where the energy of a system of localized particles is given by

$$E = -J \sum_{\langle i > j \rangle} s_i s_j, \tag{1}$$

and each particle (spin) may be in two possible states indicated by $s_i = \pm 1$. The summation includes the interaction between nearest neighbours only, indicated by $\langle i > j \rangle$. Beyond interacting spins, the Ising model is often used to approximate systems where the constituents may be in one of two possible states, describing, for example, the tunnelling between two potential wells or the occupation of a lattice site with two types of particles (Brush 1967). Ising already showed that a phase transition between an ordered state and a disordered state does not take place in this model in one dimension at non-zero temperature, whereas in two dimensions such a phase transition is possible as shown by Onsager (1944). However, extending the range of interaction beyond nearest neighbours gives rise to phase transitions even in one dimension (Gitterman and Halpern 2004).

A more sophisticated model of the interaction between localized spins (Heisenberg 1928) that, in addition, are exposed to an external local magnetic field $\vec{B}_i$ uses the Hamiltonian

$$H_s = -\frac{2}{\hbar} \sum_{i>j} J_{ij} \vec{S}_i \cdot \vec{S}_j - \frac{g \mu_B}{\hbar} \sum_i \vec{S}_i \cdot \vec{B}_i. \tag{2}$$

Here, we assume that all lattice sites are populated by particles with spin $\vec{S}_i$ with identical g-factor and eigenvalues of S_z that are multiples of $\hbar/2$ (μ_B is the Bohr magneton). No assumption has yet been made on the physical nature and range of the spin–spin coupling which is often caused by a dipole–dipole or exchange interaction. Therefore, it is useful to explicitly parametrize a possible anisotropy of this coupling by introducing the constants $J_{ij}^{(\alpha)}$, with $\alpha = x, y, z$, so that

$$H_s^{(a)} = -\frac{2}{\hbar} \sum_{\alpha=x,y,z} \sum_{i>j} J_{ij}^{(\alpha)} S_i^{(\alpha)} S_j^{(\alpha)} - \sum_i \vec{S}_i \cdot \vec{B}_i', \tag{3}$$

where the scaled local fields are defined as $\vec{B}_i' \equiv \frac{g \mu_B}{\hbar} \vec{B}_i$.

When describing physical phenomena that occur in condensed matter, for example concerning magnetism, this Hamiltonian is often subject to idealizations with regard to its dimensionality, the range of interaction, its (an-)isotropy, the uniformity of coupling constants J_{ij}, the magnitude and direction of additional (local or global) fields, and regarding the finite size of a particular system under consideration.

The Hamiltonian of the quantum transverse Ising model is obtained from $H_s^{(a)}$ for spin-1/2 particles (i.e. $\vec{S} = (\hbar/2)\vec{\sigma}$) by setting $J_{ij}^{(x)} = 0 = J_{ij}^{(y)}$ and then including further restrictions. Specifically, the local fields $\vec{B}_i$ are replaced by a global field $\vec{B} = (B, 0, 0)^T$ pointing in the x-direction, thus neglecting inhomogeneities in the physical system to be modelled (Igloi *et al* 1993, Platini *et al* 2007). Additional approximations often made are that the interaction between spins is restricted to nearest neighbours and uniform coupling $J_{ij}^{(z)} = J \, \forall i, j$ is assumed. This then leads to

$$H_{TI} = -\frac{\hbar}{2} J \sum_{\langle i > j \rangle} \sigma_i^z \sigma_j^z - B_x' \sum_i \sigma_i^x. \tag{4}$$

The quantum transverse Ising model is a prominent example for a spin model (Pfeuty 1970) that has been the starting point for many theoretical investigations (e.g. Das and Chakrabarti (2005), Part I and references therein).

2.1. Simulation of spin models with trapped ions

Using two internal states of a trapped ion as an effective spin-1/2 with the ions interacting via the Coulomb force allows for engineering spin couplings by letting the ions interact, in addition, with external dynamic and static fields. Initial theoretical and experimental work was mainly concerned with creating effective interactions between two spins to be used as two-qubit quantum gates (Cirac and Zoller 1995, 2000, Monroe *et al* 1995a, Molmer and Sorensen 1999, Milburn 1999, Milburn *et al* 2000, Sørensen and Mølmer 2000, Jonathan *et al* 2000, Jonathan and Plenio 2001, Sasura and Steane 2003, Schmidt-Kaler *et al* 2003, Leibfried *et al* 2003).

2.1.1. Direct spin–spin interaction. In this section we concentrate on couplings of the type given in equation (3) that, for example, allow us to study a phase transition between ordered and disordered phases of an ion crystal as will be outlined in section 2.2. The question we want to first consider is: how can such a spin–spin coupling be obtained in an ion trap and how can it be engineered to simulate a specific Hamiltonian?

If we consider a laser-cooled Coulomb crystal of singly charged ions confined in a linear trap such that they arrange themselves in a 1D string, then the relevant length scale for the inter-ion distance is

$$\zeta \equiv \left(e^2 / 4\pi \epsilon_0 m v_1^2 \right)^{1/3}, \tag{5}$$

where m is the mass of one singly charged ion, e is the elementary charge and v_1 is the angular vibrational frequency of the centre-of-mass (CM) axial mode of the collection of ions (Steane 1997, James 1998). We have $\zeta = 1.5 \times$

$10^{-5}(Mf^2)^{-1/3}$ m with M in atomic mass units and $f = \nu_1/2\pi$ in units of MHz. Thus, ζ typically amounts to a few micrometres. For a linear ion string, the inter-ion spacing is $\delta z \approx \zeta 2 N^{-0.56}$ (Schiffer 1993, Dubin 1993) which gives 3.7 μm for ^{171}Yb$^+$ and 9.9 μm for ^{9}Be$^+$ assuming two ions confined in a potential characterized by $f = 1$ MHz.

In principle, a direct spin–spin interaction may take place via a magnetic moment associated with the (pseudo-)spin of the ions or via an exchange interaction. However, as will be recapitulated now, the inter-ion spacing renders this interaction negligible. It is nevertheless instructive to have a look at the dipole–dipole interaction, since it may help to gain an intuitive understanding also of the *indirect* spin–spin coupling treated in section 2.1.2.

For the moment, for the sake of obtaining an intuitive picture, we consider two spins with their relative alignment fixed and exposed to local magnetic fields $B_{1,2}^{(z)}$ such that the uncoupled Hamiltonian reads as $H_0 = (\hbar/2)\big(\omega_1\sigma_1^{(z)} + \omega_2\sigma_2^{(z)}\big)$ ($\omega_{1,2}$ are the angular Larmor precession frequencies). Treating the magnetic dipole–dipole interaction as a perturbation to first order, its magnitude is determined by the expectation value

$$\langle s_1, s_2| V_{\mathrm{MD}} |s_1, s_2\rangle = s_1 s_2 f_\theta(\delta z) \equiv \pm \hbar\Delta\omega, \qquad (6)$$

where $s_{1,2} = \pm 1$ and

$$V_{\mathrm{MD}} = -\frac{\hbar^2}{4}\frac{\mu_0}{4\pi}\frac{\gamma_1\gamma_2}{\delta z^3}(3\cos^2(\theta) - 1)\sigma_1^{(z)}\sigma_2^{(z)}$$
$$\equiv f_\theta(\delta z)\sigma_1^{(z)}\sigma_2^{(z)}. \qquad (7)$$

Here, the gyromagnetic ratio of spins 1 and 2 is denoted by $\gamma_{1,2}$, μ_0 indicates the permeability of empty space and θ is the angle indicating the relative orientation of the two spins. Equation (6) tells us that the energy of the two-spin systems depends on the relative orientation between the two spins, that is, flipping either one of the two spins results in a change of energy. The physical reason is that the energy of a given spin depends not only on the imposed local field $B_{1,2}^{(z)}$, but also on the field generated by the second spin at the location of the first one, which in turn depends on its orientation (compare figures 1 and 2).

For two electron spins ($\gamma_{1,2} \approx e/m_e$ with mass m_e) and assuming $\theta = 0$, we find $\Delta\omega \approx 2\pi \times 2.6 \times 10^{-20}\delta z^{-3}$ Hz with δz measured in metres. Therefore, for a typical inter-ion separation, $\delta z = 5\,\mu$m, the direct magnetic spin–spin interaction amounts to $\Delta\omega \approx 2\pi \times 0.2$ mHz and is negligible in typical ion-trap settings. This estimate is based on a magnetic dipole–dipole interaction of ions in their ground state. If we bring the ions to a highly excited Rydberg state, one would expect an appreciable interaction between their electric dipoles (Müller *et al* 2008, Urban *et al* 2009, Gaetan *et al* 2009).

In order for the exchange interaction to play a non-negligible role, an overlap of the wavefunctions describing the external, motional degrees freedom of neighbouring ions would be required or, more precisely, the exchange integral $\int r_{12}^{-1}[\Phi_n(\vec{r}_1)\Phi_{n+1}(\vec{r}_2)]\big[\Phi_n^*(\vec{r}_2)\Phi_{n+1}^*(\vec{r}_1)\big]$ would have to have a non-negligible magnitude. Here, the spatial wavefunction of ion number n ($n + 1$) located at position $\vec{r}_1$ ($\vec{r}_2$) is $\Phi_n(\vec{r}_1)$ ($\Phi_{n+1}(\vec{r}_2)$) and the integration is carried out over all space. However, the root mean square extension of the ground-state
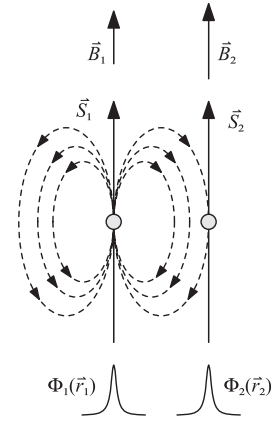
Figure 1. An artist's illustration of the coupling between two spins via a dipole–dipole interaction. Two classical magnetic moments $\gamma_i\vec{S}_i$ fixed in space are exposed to individual external magnetic fields $\vec{B}_i$ ($i = 1, 2$) that determine their respective energy for a given orientation (parallel or anti-parallel to $\vec{B}_i$). Spin-2 experiences in the presence of spin-1, in addition to $\vec{B}_2$, an additional field that depends on the relative orientation between the two spins. Thus, the energy of spin-2 is shifted depending on the orientation of spin-1 (and vice versa). The spatial wavefunctions of the two spins are indicated by $\Phi_i(\vec{r}_i)$.
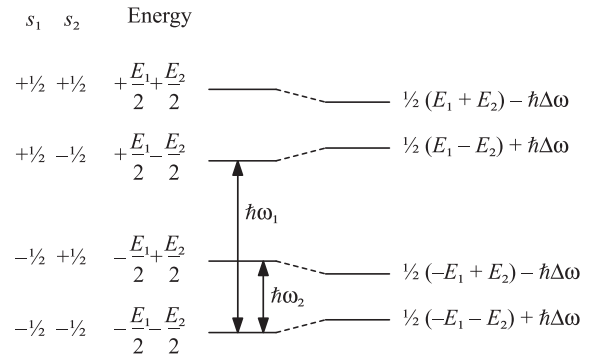

Figure 2. Energy levels of two spins as a function of their orientation. The quantum numbers s_i, $i = 1, 2$, indicate the spin state. The resonance frequencies of non-interacting spins are ω_i while when they interact these resonances are shifted by $\Delta\omega_i$.

wavefunction of a trapped ion is given by $\Delta z_1 = \sqrt{\hbar/2m\nu_1} = 7.1 \times 10^{-8} \times (Mf)^{-1/2}$ m. In the case of a ^{9}Be$^+$ (^{171}Yb$^+$) ion, one obtains $\Delta z_1 = 24$ nm (5.4 nm) for $f = 1$ MHz which typically is three orders of magnitude smaller than the inter-ion separation δz. Therefore, the exchange interaction can be neglected, too.

2.1.2. Spin–spin interaction mediated by the Coulomb force. Thus, a direct spin–spin interaction between trapped ions will not be sufficiently strong for a useful implementation of the spin models described above. Instead, we now look for an interaction that is mediated by some other physical mechanism.

Physical picture. The applied trapping potential and the Coulomb forces between the ions determine their equilibrium positions. Now, by applying a suitable external field, an
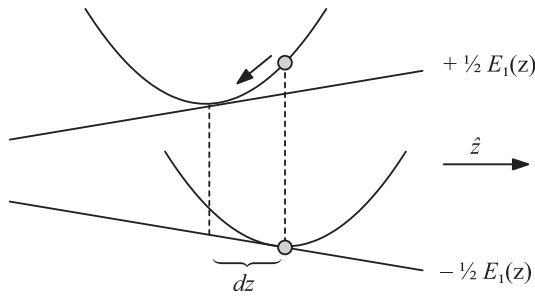
Figure 3. A single ion confined in a potential that is the sum of a harmonic oscillator and a linear term. The sign of the linear term depends on the internal spin state ($\pm\frac{1}{2}E_1$) of the ion. Upon flipping the ion's spin, its motion can be excited.

Figure 4. Sketch of two ions confined in a harmonic potential with a superimposed spatially varying magnetic field $\vec{B}$ to illustrate spin–spin coupling mediated by Coulomb repulsion. When we flip the spin of ion 1, the state-dependent force acting on it will change sign and, thus, its equilibrium position will change ($1 \rightarrow 1'$). Through Coulomb interaction the second ion, too, will change its equilibrium position ($2 \rightarrow 2'$), and, since it moves in a field gradient, consequently will change its internal resonance frequency from ω_2 to ω_2'.

additional force is exerted on each ion whose magnitude and/or direction depend on the orientation of the spin of the ion and vary spatially (i.e. depend on the exact location of the ion). If this state-dependent force acts in addition to the trap and Coulomb forces, then a spin flip of ion 1 changes this force and, as a consequence, this ion changes its equilibrium position. Via Coulomb repulsion, this in turn leads to a shift of the equilibrium position of the neighbouring ion 2 that now finds itself exposed to a field of different magnitude and thus changes its internal energy.
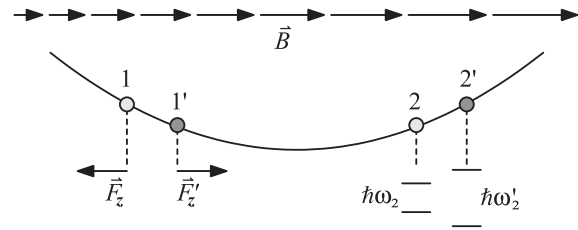
This additional field may be a static magnetic field with spatially varying magnitudes. The direct interaction between magnetic dipoles (where flipping one spin amounts to a change in the local magnetic field experienced by another nearby spin) is replaced by an indirect interaction where the change in the magnetic field at the location of spin-2 is brought about by a change of its equilibrium position (caused by the spin flip of ion 1) in a spatially varying external field.

For a more quantitative description, we consider the force $\vec{F} = \langle(\vec{\mu} \cdot \vec{\nabla})\vec{B}\rangle$ acting on an atomic magnetic moment $\vec{\mu} = (\gamma\hbar/2)\vec{\sigma}$ associated with spin $(\hbar/2)\vec{\sigma}$ in a magnetic field $\vec{B}$. Without loss of generality, we restrict the following discussion to the case where $\vec{B} = \vec{B}_0 + b\hat{z}$ with constant offset field $\vec{B}_0$ and gradient b along the z-axis[1] such that the force $F_z = \langle(\gamma\hbar/2)b\sigma^{(z)}\rangle$ changes sign upon flipping the atomic spin ($\langle\rangle$ indicates the expectation value). Using the position-dependent spin resonance frequency $\omega = \gamma bz$, the force can be expressed as a function of the change of ω when moving the ion along the z-axis:

$$F_z = (\hbar/2)\partial_z\omega\langle\sigma^{(z)}\rangle. \qquad (8)$$

For an ion of mass m confined in a harmonic potential, characterized by angular frequency ν, this linear force that acts in addition to the trapping potential and Coulomb force shifts the equilibrium position of the ion, upon flipping its spin, by an amount $d_z = \mp F_z/(m\nu^2)$ from its initial equilibrium position (compare figure 3). Thus, in a classical picture, the ion finds itself on the slope of a harmonic oscillator potential, instead of at the potential minimum, after its spin was flipped. Consequently, it will start to oscillate around the new

equilibrium position. In this way the ion's internal dynamics and its motional degrees of freedom can be coupled, even if the radiation causing the spin flip does not impart enough linear momentum to excite the ion's motion. This coupling, quantum mechanically described by an effective Lamb–Dicke parameter $\eta_{\text{eff}} = d_z/\Delta z$ (Mintert and Wunderlich 2001, 2003, Wunderlich 2002, Wunderlich and Balzer 2003), has been recently observed experimentally (Johanning *et al* 2009).

In order to see how the desired J-coupling (see equation (3)) arises, we consider how an ion's shift of its equilibrium position affects its internal energy. This change of its internal energy is given by

$$\hbar J = -F_z d_z = -F_z^2/(m\nu^2) \propto (b/\nu)^2. \qquad (9)$$

As a consequence of one ion's shift of equilibrium position, through Coulomb interaction, the position and energy of neighbouring ions are shifted, too, giving us the desired (indirect) spin–spin interaction (compare figure 4).

Calculation of spin–spin coupling. After having introduced this general physical mechanism that may be used to induce an effective spin–spin interaction, we will now briefly outline how this may be employed to engineer a variety of interactions between a collection of trapped ions. We consider the internal energies of N ions all of which experience a shift of their internal resonance frequency that, for now, depends on their axial position denoted by z, only:

$$H_I = -\frac{\hbar}{2}\sum_{n=1}^{N}\omega_n\sigma_z^{(n)} - \frac{\hbar}{2}\sum_{n=1}^{N}\partial_z\omega_n q_n\sigma_z^{(n)} \qquad (10)$$

Here, q_n is the deviation of ion n from its equilibrium position $z_n^{(0)}$,

$$\omega_n \equiv \omega|_{z_n^{(0)}}, \; \partial_z\omega_n \equiv \partial_z\omega|_{z_n^{(0)}}, \qquad (11)$$

and the expansion of ω_n has been included up to first order[2].

The external (motional) degrees of freedom of N ions are determined by the applied trapping potential and their mutual

---

[1] Such a field may be *approximately* realized, even though it does not fulfil $\vec{\nabla}\cdot\vec{B} = 0$, for example, on the axis of rotational symmetry of a quadrupole field sufficiently far from the point of inflection symmetry.

[2] We assume a constant field gradient, that is, second-order and higher order derivatives of the field vanish. However, expression (10) is still valid even if these derivatives are different from zero as long as the *gradient* does not vary appreciably over the extent Δz of an ion's spatial wavefunction.

Coulomb repulsion. Expanding the total potential up to second order gives

$$V^{(\text{harm})} = \frac{m}{2} \sum_{\alpha=1}^{3} \sum_{i,j=1}^{N} A_{\alpha\alpha,ij} q_{\alpha,i} q_{\alpha,j}, \tag{12}$$

where the three spatial degrees of freedom $\alpha = x, y, z$ are uncoupled (James 1998). The Hessian matrices $A_{\alpha\alpha,ij}$ that characterize the potential experienced by the ions are real valued and symmetric in i and j and are transformed into diagonal matrices D_α via $D_\alpha = S_\alpha^{-1} A_\alpha^{(2)} S_\alpha$ with eigenvectors $\vec{Q}$.

In terms of the normal coordinates, we obtain the following Hamiltonian describing $3N$ uncoupled harmonic oscillators (James 1998):

$$H_{\text{E}} = \sum_{\alpha=1}^{3} \left[\frac{1}{2m} \sum_{n=1}^{N} P_{\alpha,n}^2 + \frac{m}{2} \sum_{n=1}^{N} \nu_{\alpha,n}^2 Q_{\alpha,n}^2 \right], \tag{13}$$

where $\nu_{\alpha,n}$ is the angular frequency of the normal vibrational mode n in direction $\alpha = x, y, z$ and the relation between the normal coordinates $Q_{\alpha,n}$ and the local coordinates $q_{\alpha,n}$ is $\vec{Q}_\alpha \equiv (Q_{\alpha,1}, \ldots, Q_{\alpha,N}) = S_\alpha^{-1} \vec{q}_\alpha$ with $\vec{q}_\alpha = (q_{\alpha,1}, \ldots, q_{\alpha,N})$; furthermore, $P_{\alpha,n} \equiv m \dot{Q}_{\alpha,n}$.

The total Hamiltonian includes internal and motional parts $H = H_{\text{I}} + H_{\text{E}}^{(z)}$, where, for now, we restrict our considerations to the spatial z-direction where a field gradient is present. If a magnetic field gradient was present also in the radial direction (which is the case, e.g., for a quadrupole field close to its point of symmetry), then the radial vibrational modes would also contribute to the J-coupling. However, this contribution is usually small, since in order to maintain a linear ion string, the angular frequencies $\nu_{x,1}$ and $\nu_{y,1}$, characterizing the radial trapping potential, are usually chosen much larger than $\nu_{z,1}$. Taking into account that the J-coupling is proportional to the inverse square of the trap frequency (taking equation (9) as a guideline), we neglect the contribution from transverse vibrational modes for now. In Porras and Cirac (2004a) and Deng *et al* (2005), transverse modes are explicitly considered (see below).

After expressing the local coordinates q_n in equation (10) by the normal coordinates, $q_n = \sum_{l=1}^{N} S_{nl} Q_l$, noting that $Q_l = \Delta z_l (a_l^\dagger + a_l)$, $P_l = i m \nu_l \Delta z_l (a_l^\dagger - a_l)$ and performing a suitable unitary transformation of H, $\tilde{H} = U^\dagger H U$, with

$$U \equiv \exp\left(-\frac{i}{\hbar} \sum_{n,l=1}^{N} \Delta z_l \varepsilon_{nl} \sigma_z^{(n)} P_l \right), \tag{14}$$

we obtain (Wunderlich 2002)

$$\tilde{H} = -\frac{\hbar}{2} \sum_{n=1}^{N} \omega_n \sigma_z^{(n)} + \hbar \sum_{n=1}^{N} \nu_n a_n^\dagger a_n - \frac{\hbar}{2} \sum_{\substack{i,j=1 \\ i<j}}^{N} J_{ijl} \sigma_z^{(i)} \sigma_z^{(j)}, \tag{15}$$

where the vibrational motion and the internal states are now decoupled ($a_n^\dagger$ and a_n are respectively the creation and annihilation operators of vibrational mode n). The spin–spin coupling constants are given by

$$J_{ij} \equiv \sum_{n=1}^{N} \nu_n \varepsilon_{in} \varepsilon_{jn}, \tag{16}$$

where the dimensionless constants

$$\varepsilon_{in} \equiv \frac{\Delta z_n \partial_z \omega_i}{\nu_n} S_{in} \tag{17}$$

have been introduced. The numerator of the fraction on the right-hand-side of equation (17) gives the change of the internal energy (or frequency) that ion number i undergoes when its position is shifted by an amount equal to the extension of the ground-state wavefunction, $\Delta z_n = \sqrt{\frac{\hbar}{2m\nu_n}}$, of vibrational mode n. This is set in relation to the energy (frequency) of a phonon of mode n. The matrix element S_{in} gives the scaled deviation of ion i from its equilibrium position when vibrational mode n is excited. Thus, ε_{in} tells us how strongly ion number i couples to vibrational mode n when its spin is being flipped. The sum in equation (16) extends over all vibrational modes, since the local deviation, q_n, of ion i from its equilibrium position potentially (if S_{in} is different from zero) excites all vibrational modes of the ion string.

Noting that $\nu_n \propto \nu_1$ and $F_{z,i} \propto \partial_z \omega_i$ and plugging the expression for Δz into equation (17), we find from equation (16) that

$$J_{ij} \propto \frac{F_{z,i} F_{z,j}}{\nu_1^2} \propto \left(\frac{b}{\nu_1} \right)^2 \tag{18}$$

in agreement with the result (9) that was found from a simple model based on classical considerations (here, ν_1 is the angular frequency of the centre-of-mass mode of N ions). One obtains the proportionality between the second and third terms in relation (18), if the state-dependent force is caused by a constant magnetic field gradient (that gives rise to a linear Zeeman shift of the spin states of ions i and j).

This spin–spin coupling is only weakly sensitive to thermal excitation of the ion string. Thus, usually simple Doppler cooling will be sufficient to avoid unwanted thermal effects on the coupling constants J_{ij} (Loewen and Wunderlich 2004). Detailed calculations on this aspect will be published elsewhere.

In Ospelkaus *et al* (2008), it is shown how an *oscillating* magnetic field generated in a micro-structured surface trap may be used to induce spin coupling between ions and how this could be employed to carry out quantum gates.

Spin–spin interaction created by an optical force. The J-coupling described above may also be created by a state-dependent *optical* force (instead of the magnetic force assumed above) induced by an off-resonant standing laser wave (Porras and Cirac 2004a, Deng *et al* 2005). Applying state-dependent forces (e.g. optical or magnetic forces) along different spatial directions, combined with various trapping conditions, a variety of different coupling Hamiltonians of the general form

$$H_s^{(\text{ion})} = -\frac{1}{2} \sum_{\alpha=x,y,z} \sum_{i>j} J_{ij}^{(\alpha)} \sigma_i^\alpha \sigma_j^\alpha - \sum_i \sigma_i^\alpha \vec{B}_i^{\alpha'} \tag{19}$$

may be realized (Porras and Cirac 2004a, Deng *et al* 2005).

In particular, in Deng *et al* (2005) it is shown how state-dependent forces that act in the radial direction of a 1D ion string may be exploited to simulate a transverse quantum Ising model and an XY model, either with Coulomb crystals confined by a global potential or with linear arrays of

J. Phys. B: At. Mol. Opt. Phys. **42** (2009) 154009

Review

microtraps where each ion is confined in its own, externally controlled potential well. It is demonstrated (by means of numerical and analytical calculations) under which conditions quantum phase transitions should be observable with 1D strings of trapped ions, and what the expected characteristic features of these transitions are, as compared to the usual Ising and XY models where only nearest-neighbour interaction is considered.

2.1.3. Engineering the spin–spin coupling. A straightforward way to apply a magnetic gradient that induces the long-range J-coupling described above in a linear Coulomb crystal is the use of current-carrying coils in an anti-Helmholtz-type arrangement, mounted such that their axis of rotational symmetry coincides with the trap z-axis. The field generated by these coils is easily calculated analytically and gradients up to several tens of T m^{-1} are attainable with coils with a diameter of typically 1 mm. Some examples for possible configurations and computed examples for J-coupling constants are presented in Wunderlich and Balzer (2003), Wunderlich *et al* (2005) and Wunderlich and Wunderlich (2009). Such coils may also be integrated into micro-structured ion traps that are currently being developed. Here, larger gradients are realistic (several hundreds of T m^{-1}) (Brüser, submitted). When using current-carrying structures for generating magnetic fields, the currents, and thus the J-coupling, can be turned on and off as required; however, the stability of the magnetic field needs attention to avoid dephasing of spins. Alternatively, permanent magnets may be used (Johanning *et al* 2009).

Global trap potential. If the ions are confined in one common trapping potential, then the strength of the J-coupling may be controlled globally, that is, all coupling constants may be varied together by adjusting the gradient b and/or the secular trap frequency ν_1. In a linear Paul trap the trap frequency along the z-axis of a linear trap is adjustable by applying a suitable voltage to the end cap electrodes, while the radial trapping frequency can be adjusted by varying the amplitude of the applied rf trapping field. If the gradient b is generated by electrical currents, then these currents can be varied, and turning the magnetic field on and off using a desired envelope allows for simultaneous switching of all coupling constants. If permanent magnets are used, and their position is fixed along the z-axis (typically generating a quadrupole field), the ions may be moved collectively along the z-axis to change the gradient they experience. Moving the ions in a linear Paul trap is achieved by applying suitable voltages to the electrodes that are responsible for the axial confinement. Even an always-on interaction (that arises, for instance, when using permanent magnets to generate a field gradient) used in conjunction with coherent manipulation of individual spins may be employed such that prescribed entangled states can be generated in a time-optimal way (Fisher, private communication) for the axial confinement.

Locally variable trap potential. The advent of micro-structured traps brings with it the possibility of attaining

control over local trapping potentials and thus of engineering the J-coupling locally. For example, employing a linear Paul trap with dc electrodes that are segmented such that individual electrodes have an axial extension of the order of the inter-ion separation allows for shaping the local electrostatic potential such that long-range coupling is strongly suppressed and essentially only uniform nearest-neighbour coupling exists (Hugh and Twamley 2005).

Furthermore, micro-structured traps with segmented electrodes allow for detailed local sculpting of J-coupling constants. This can be useful to generate effective time evolution operators making it possible to reach a desired entangled state in a single time evolution step without the need for refocusing. Examples of how to generate cluster states in this way are given in Wunderlich and Wunderlich (2009).

A possible drawback of the use of small electrodes is that this usually implies an equally small distance between ions and nearby surfaces (i.e. typically of order 10 μm) which leads to high heating rates of the ions' secular motion and thus limits the useful time available for coherent dynamics (Turchette *et al* 2000). Using ion traps embedded in a cryogenic environment considerably reduces this heating rate (Deslauriers *et al* 2006, Labaziewicz *et al* 2008) and, therefore, may provide a feasible approach to using small electrode structures. A micro-fabricated linear surface trap cooled to 4 K that includes current-carrying structures for generating a magnetic field gradient was recently demonstrated (Wang *et al* 2008). The magnetic gradient was used to address individual ^{88}Sr$^+$ ions in frequency space on an optical transition between Zeeman states of the electronic ground state $5S_{1/2}$ and the metastable state $4D_{5/2}$, respectively.

Segmented ion traps also allow for transporting ions between different trap locations (Wineland *et al* 1998, Kielpinski *et al* 2002, Rowe *et al* 2002, Home and Steane 2006, Hensinger *et al* 2006, Schulz *et al* 2006, Reichle *et al* 2006, Hucul *et al* 2008, Huber *et al* 2008). For moving ions, the required electrode structures may be considerably larger, typically of order 100 μm, thus helping to reduce unwanted heating. The transport of ions over small distances in segmented ion traps gives a further handle to engineer effective couplings by letting only a subset of ions interact at a time in a prescribed way. This could be used, for example, to generate two-dimensional cluster states using a one-dimensional linear Coulomb crystal (Wunderlich and Wunderlich 2009).

A possible architecture for a two-dimensional surface trap array exploiting a magnetic field-gradient-induced spin–spin coupling as described above was proposed in Chiaverini and Lybarger (2008). In Clark *et al* (2008), confinement of ^{88}Sr$^+$ ions in a 2D ion-trap array with individual sites spaced apart by about 1.6 mm is reported. Even though a trap array with such a large inter-ion spacing does not allow for a useful spin coupling between the ions, it is nevertheless useful as a proof-of-principle and makes possible the investigation of the scaling behaviour of this trap array. It turns out that scaling down of the layered rf lattice trap alone is unlikely to be a promising route to achieve useful J-coupling. It appears that further modifications of this trap design are useful to ensure low enough secular frequencies for sufficiently strong J-coupling (compare equation (18)).

Recently, two-dimensional and linear arrays of Penning traps that confine individual electrons have been proposed as a promising physical system for quantum computation and quantum simulations. Here, the physical origin of the J-coupling is again a force that depends on an electron's spin state and is caused by a magnetic field gradient and, as in ion traps, the Coulomb force between electrons mediates the spin–spin coupling (Stahl *et al* 2005, Ciaramicoli *et al* 2005, 2007, 2008). Thus, various couplings as in equation (3) with variable ranges could be realized with trapped electrons and used, for instance, to investigate quantum phase transitions.

2.1.4. Simulating an effective transverse field. An effective transverse magnetic field can be simulated by driving transitions between the spin states of ion i employing a radio frequency or optical field resonant with this ion's qubit transition[3]:

$$H_t = -\hbar \Omega_R \cos(\omega^{(i)} t + \phi') \sigma_x^{(i)} \tag{20}$$

$$= -\frac{\hbar}{2} \Omega_R (\sigma_+^{(i)} + \sigma_-^{(i)})(e^{i(\omega^{(i)} t + \phi')} + e^{-i(\omega^{(i)} t + \phi')}). \tag{21}$$

Here, Ω_R is the Rabi frequency that for a linearly polarized rf field $B_x \cos(\omega_x t + \phi')$ reads as $\Omega_R = \gamma B_x / 2$ and the resonance condition is $\omega_x = \omega^{(i)}$.

First transforming H_t by U, as was done above for the Hamiltonian H (equations (14) and (16)), then carrying out a transformation into an interaction picture with respect to $-\frac{\hbar}{2} \sum_{n=1}^{N} \omega_n \sigma_z^{(n)} + \hbar \sum_{n=1}^{N} \nu_n a_n^\dagger a_n$ (Wunderlich 2002), expanding the resulting Hamiltonian up to first order in $a^\dagger$ and a, neglecting terms that contain ε_{in}[4] and applying the rotating wave approximation, one obtains for spin i

$$\tilde{H}_t^{(i)} = -\frac{\hbar}{2} \Omega_R (\sigma_x^{(i)} \cos\phi - \sigma_y^{(i)} \sin\phi) \tag{22}$$

when the rf field or optical field is on resonance. Allowing for a detuning $\omega_{rf} - \omega^{(i)}$ between the applied field and the spin-flip resonance frequency introduces a term proportional to $(\omega_{rf} - \omega^{(i)}) \sigma^{(z)}$ on the rhs of equation (22). Thus, by driving spin transitions of individual ions, a variety of additional local effective magnetic fields $\vec{B}_n' \propto (\cos\phi_n, -\sin\phi_n, (\omega_{rf} - \omega^{(n)})^T$ in Hamiltonian (3) may be simulated. In particular, by choosing the phase ϕ' of the rf field such that $\phi = 0$ and fulfilling the resonance condition for all ions, a global transverse field B_x' for the transverse Ising model (4) is implemented.

2.1.5. Spin-boson model. The spin-boson model ((Leggett *et al* 1987, Weiss 1999) and references therein) is the starting point for the modelling of many theoretical investigations, for instance the decoherence of a variety of physical systems. It describes the dynamics of a spin-1/2 coupled to a bath of harmonic oscillators that represent the spin's environment. Thus, the spin-boson Hamiltonian contains a term proportional to σ_z (describing the spin's energy), a term proportional to

σ_x (describing spin flips), a term describing the harmonic oscillators, $\hbar \sum_l \nu_l (a_l^\dagger a_l + 1/2)$, and finally a term coupling the spin to the oscillators

$$\frac{\hbar}{2} \sigma_z \sum_l C_l Q_l, \tag{23}$$

where Q_l is the position coordinate of the lth harmonic oscillator while C_l describes the coupling strength between this oscillator and the spin. We note that all these ingredients are already present in the formulae presented above: Picking out a particular ion i, equation (10) may be rewritten as

$$H_I^i = -\frac{\hbar}{2} \omega_i \sigma_z^{(i)} - \frac{\hbar}{2} \sigma_z^{(i)} \sum_{n=1}^{N} \partial_z \omega_i q_n$$
$$= -\frac{\hbar}{2} \omega_i \sigma_z^{(i)} - \frac{\hbar}{2} \sigma_z^{(i)} \sum_{l=1}^{N} \partial_z \omega_i \left(\sum_{n=1}^{N} S_{nl} \right) Q_l \tag{24}$$

and we can set $C_l = \partial_z \omega_i \left(\sum_{n=1}^{N} S_{nl} \right)$ to obtain in equation (23) the coupling between spin i and the harmonic oscillators represented by the collective vibrational modes of a string of N ions. The term proportional to σ_x required for the spin-boson model is obtained by driving transitions between the two spin orientations (see above, equation (22)).

Now the question arises how to physically single out a particular spin i from the sum over all spins in the second term of H_I (equation (10)) such that we are left with H_I^i in equation (24). This could be done by exerting a state-dependent force only on ion i as is shown in Porras *et al* (2008). Porras *et al* detailed how laser beam(s) focussed onto one particular ion gave rise to optical forces that induce the required coupling. Furthermore, it is shown how phonon baths characterized by a variety of spectral densities may be simulated and how effects caused by the finite size of the ion crystal may be observed.

2.2. Phase transition

2.2.1. Quantum transverse Ising model. The quantum transverse Ising model (TIM, equation (4)) already displays a phase transition in one dimension (Sachdev 1999), even at zero temperature, between an ordered state and a disordered state upon varying B_x'/J. Milburn (1999) and Milburn *et al* (2000) proposed an implementation of a unitary map closely related to the TIM using Raman laser pulses. In Porras and Cirac (2004a), it is proposed how to observe this QPT with trapped ions interacting with a standing laser wave that creates a long-ranged spin coupling as outlined above (section 2.1.2). Barjaktarevic *et al* (2005) proposed to implement a unitary map that displays a QPT belonging to the same universality class as the transverse Ising model.

In order to get a qualitative picture of such a phase transition, we first consider the collection of spins described by H_{TI} (equation (4)) in the limit where the effective transverse field, B_x', assumes a finite value, but the mutual coupling J between spins vanishes, $B_x' \neq 0 = J$, such that, at zero temperature, all spins are oriented along the x-direction and the ground state $|0\rangle = \prod_i |\rightarrow\rangle_i = \prod_i (|\uparrow\rangle_i + |\downarrow\rangle_i)$ of the system is a product of eigenstates of σ_i^x. Consequently,

---

[3] Optical fields may be used to drive transitions not only in the optical range, but also in the rf range by applying a two-photon Raman excitation.
[4] In Deng *et al* (2005), the effects of residual spin–phonon coupling caused by the effective transverse field are calculated.

$\langle 0| \sigma_i^z \sigma_j^z |0\rangle = \delta_{ij}$, that is, the orientation of different spins with respect to the the z-axis is uncorrelated. On the other hand, if the spin–spin coupling does not vanish, $B_x' \gg |J| > 0$, the spins will acquire a tendency to align along the z-axis. Thus, the ground state of the system will start to exhibit non-vanishing, but short-ranged, correlations between spins located at sites r_i and r_j, respectively, with a characteristic length scale ξ (Sachdev 1999):

$$\langle 0| \sigma_i^z \sigma_j^z |0\rangle \propto e^{-|r_i - r_j|/\xi}. \tag{25}$$

Here, $|0\rangle$ is the system's ground state when $B_x' \gg |J| \neq 0$.

Now, we turn to the limit $B_x' \ll J > 0$. If B_x' vanishes completely, then an infinite system of spins possesses two degenerate ferromagnetic ground states where all spins are either parallel or anti-parallel to the z-axis and the total magnetization of the system is M_0. Turning on a small field $B_x' \ll J$ pointing in the x-direction will tend to reorient some of the spins along the x-direction (classically, their magnetic moments will start to precess around the x-direction, thus flipping spins between the two possible z-orientations). The ground state of the system, $|0\rangle$, is still close to the $B_x' = 0$ case and is obtained from a perturbative expansion in the small parameter B_x'/J. One finds $\langle 0| \sigma_i^z |0\rangle = M/M_0$ where $M < M_0$ is now the spontaneous magnetization of the system. Again calculating the correlation of the orientation of different spins in the z-direction for this ground state gives (Sachdev 1999)

$$\lim_{|r_i - r_j| \to \infty} \langle 0| \sigma_i^z \sigma_j^z |0\rangle = \left(\frac{M}{M_0}\right)^2. \tag{26}$$

Expressions (25) and (26) for the spin correlation are incompatible in the sense that a continuous variation of B_x'/J between the two limiting cases considered above does not allow for an analytical connection between the two expressions on the right-hand sides of equations (25) and (26). Thus, there must exist a critical value of B_x'/J where the correlation changes between these two expressions. This is the case even at zero temperature being indicative for a quantum phase transition.

An experimental realization of the proposal by Porras and Cirac (2004a) with two trapped and laser-cooled ^{25}Mg$^+$ ions was recently reported by Friedenauer *et al* (2008). Here, the coupling J between spins is induced by a state-dependent ac-Stark shift caused by a 'walking' standing wave. Two hyperfine states of the electronic ground state of each ^{25}Mg$^+$ ion served as an effective spin-1/2 with eigenstates $|\downarrow\rangle$ and $|\uparrow\rangle$. In brief, the experimental procedure is as follows. Optical pumping is employed to first initialize the two ions in state $|\downarrow, \downarrow\rangle$. Resonantly driving the transition between the two hyperfine states with rf radiation simulates an effective transverse field B_x' (section 2.1.4) and allows for preparation of the initial paramagnetic state $|\rightarrow, \rightarrow\rangle$ (both spins are oriented along the effective B_x' field). Then, the J-coupling between the two spins is ramped up adiabatically from zero to a desired value such that the ratio $J/B_x' \leqslant 5.2$. For $J \gg B_x'$ one expects that the two spins are found in a ferromagnetic state, that is, aligned along the z-axis. In general, the new ground state will be a superposition of the states $|\downarrow, \downarrow\rangle$ and $|\uparrow, \uparrow\rangle$ which

is indeed found experimentally. In a further experiment the two spins were prepared initially anti-parallel to the effective B_x' field, an excited paramagnetic state. Turning on the spin–spin coupling adiabatically then resulted in an excited state in the presence of strong J-coupling ($J/B_x' \gg 1$): the anti-ferromagnetic state $|\uparrow, \downarrow\rangle + |\downarrow, \uparrow\rangle$. In both cases, the entanglement of the final state was proven experimentally.

2.2.2. Scalar fields. Classical phase transitions between spatial configurations of ions confined in a linear or ring-shaped trap have been investigated experimentally and theoretically (Waki *et al* 1992, Raizen *et al* 1992, Birkl *et al* 1992, Dubin 1993, Schiffer 1993, Drewsen *et al* 1998, Kjærgaard and Drewsen 2003, Morigi and Fishman 2004a, 2004b, Fishman *et al* 2008). Retzker *et al* (2008) suggested to explore a phase transition between a linear and a zigzag configuration (Fishman *et al* 2008) in the quantum regime, that is, with the ion string cooled close to its vibrational ground state. The ion-trap parameters are chosen such that a linear Coulomb crystal forms (i.e. the confinement in the axial direction is weaker than in the radial direction) and, in addition, $\nu_{y,1} \gg \nu_{x,1}$ such that one radial degree of freedom is essentially frozen out after laser cooling, but the other may be employed for quantum simulations. Linear Paul traps as well as Penning traps where the ions are confined on the axis of rotational symmetry (Powell *et al* 2002) are well suited for this purpose.

For $\nu_{1,x}$ below a critical value $\nu_{1,x}^c$, a zigzag configuration of the ions will form with two degenerate states. It is shown in Retzker *et al* (2008) that coherent tunnelling between these two states may be observed and used for interferometry. Furthermore, by adjusting $\nu_{1,x}$ around $\nu_{1,x}^c$ the parameters of a Hamiltonian describing the ions' motional excitation along the x-direction may be determined. This Hamiltonian describes at the same time a nonlinear scalar field and by adjusting $\nu_{1,x}$ the effective mass of this field may be varied, in particular in the vicinity of a phase transition. An attractive feature of this proposal is that *global* adjustment of the radial trapping frequency $\nu_{1,x}$ is sufficient and no local control over the trapping potential is needed.

2.3. Neural network

In Pons *et al* (2007) and Braungardt *et al* (2007), it was shown that a linear Coulomb crystal of laser-cooled trapped ions may be used to implement a neural network (NN)—according to the Hopfield model (Hopfield 1982)—allowing for robust storage of classical information and, furthermore, that such a NN may be employed for error-resistant quantum computation. We will first briefly introduce some features of the Hopfield model (see, e.g., Rojas (1996), chapter 13 and references therein) and then outline how some features may be realized with trapped ions.

A neural network according to the Hopfield model consists of N nodes (corresponding to neurons) that are all mutually interconnected and we indicate the (synaptic) strength of the connection between node i and node j by J_{ij}. This connection is symmetric, that is, $J_{ij} = J_{ji}$ and the nodes do not feed back to themselves, $J_{ii} = 0$. Below, we will see what
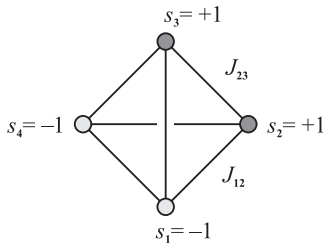
Figure 5. Illustration of a neural network that consists of four nodes according to Hopfield (1982). Each node may exist in one out of two states indicated by $s_i = \pm 1$, $i = 1, 2, 3, 4$. The nodes are all interconnected with $J_{ij} = J_{ji}$. Here, the network forms a pattern $\vec{\xi} = (-1, +1, +1, -1)^T$. (Note that the number p of patterns that can be stored by a Hopfield network is about $p = 0.14N$, where N is the number of nodes.)

exactly the meaning of the coupling strengths J_{ij} is. Each node can assume one of two possible states which we label by $s_i = \pm 1$ (compare figure 5). When modelling neurons, this would indicate whether the neuron is 'firing' (a sudden change of a biologically relevant potential difference) or in a quiescent state at a given time. Furthermore each node is characterized by a threshold h_i that, in addition to the couplings J_{ij}, influences its response to the input from other nodes.

A characteristic feature of a Hopfield NN is that it can store information distributed over all nodes. Thus, it is robust against errors in individual nodes or even the loss of some nodes and against thermal noise. The dynamics of the NN, being determined by the strengths of interactions between all nodes, brings the system back to one out of a selection of particular states (that we call patterns) once this state was disturbed. This feature may be taken advantage of for pattern recognition. When the NN is presented with some input state, which is done by initializing all nodes with a given value, then the NN evolves into the pattern that it was trained to recognize that is closest to this initial state. So how does the NN dynamically evolve?

We start at time t with an initial global state of the NN labelled by the N-component vector $\vec{s}$ where each local node is characterized by s_i. Then the state of each node at time $t + \delta t$ is determined by the sign of the activation function A at time $t + \delta t$:

$$s_i(t + \delta t) = \text{sgn}(A(t + \delta t)), \qquad (27)$$

where

$$A(t + \delta t) = \sum_{j \neq i} J_{ij} s_j(t) + h_i. \qquad (28)$$

This means that at time $t + \delta t$, node i will be firing ($s_i = +1$) or in a quiescent state ($s_i = -1$) depending on the state of all other nodes at time t, weighted with the strength J_{ij}, and the individual threshold h_i. One of the two following alternative model assumptions is usually made: the updating of node i may either occur sequentially, one node after the other, or in parallel all at the same time.

We now define the cost function

$$H_H(\vec{s}) = -\frac{1}{2} \sum_{i, j (i \neq j)} J_{ij} s_i s_j - \sum_i h_i s_i \qquad (29)$$

and it can be shown (Rojas 1996) that an evolution of the network according to the dynamical rule for sequential updating (27) (together with definition (28)) leads to a monotonic decrease of H_H[5]. This means that flipping spins (in agreement with the rules) drives the system towards local or global minima in the 'landscape' defined by H_H over the space of $\vec{s}$.

We immediately realize that the expression defining H_H is formally equivalent to the spin Hamiltonian H_s (equation (3)) considering the case of spin-1/2 particles with $J_{ij}^{(x)} = 0 = J_{ij}^{(y)}$. As noted at the beginning of the section on spin models, further simplifications of H_s, namely uniform J-coupling, only nearest-neighbour interaction, and no transverse field lead to the Ising model (equation (1)). When considering the Ising model, one usually assumes that all coupling constants are positive or all are negative and thus arrives at a limited set of minima (e.g. for $J > 0$, all spins are all either up or down). However, here the couplings J_{ij} are not restricted to being all positive or all negative, thus allowing for a rich 'energy landscape' with many minima.

Our goal is to 'teach' the NN a specific pattern, $\vec{\xi}$, $\xi_i = \pm 1$ towards which the NN is supposed to relax, if it is displaced from this pattern or if presented with a similar input pattern. In other words, this pattern must correspond to a minimum of H_H. Where exactly this minimum occurs, that is, for which particular configuration $\vec{s}$, is determined by the choice of the interaction strengths J_{ij}. Therefore, if one wants the NN to 'remember' a particular pattern $\vec{\xi}$ (i.e. create a minimum of H_H for a specific arrangement $\vec{\xi}$ of the nodes), the J-couplings need to be adjusted accordingly. At first sight (and probably still at second), it is not obvious how a set of J-couplings may be found that creates a minimum of H_H for a desired pattern and thus makes the NN evolve towards this pattern. It turns out that using Hebb's rule (Hebb 1949, Mezard *et al* 1987) to determine the values of the couplings J_{ij} gives just the right set of J-couplings.

In order to memorize a pattern $\vec{\xi}$, each J_{ij} is modified according to Hebb's rule of learning, such that

$$J_{ij}^{\text{new}} = \lambda J_{ij}^{\text{old}} + \epsilon \xi_i \xi_j. \qquad (30)$$

When we start with an 'empty' memory, then $J_{ij}^{\text{old}} = 0$. In the original Hopfield model, $\lambda = 1 = \epsilon$; another choice is $\epsilon = 1/N$. With the set of interconnections, J_{ij} determined by equation (30) the NN, upon turning on its dynamics, will eventually end up in the memorized pattern $\vec{\xi}$. If the NN is supposed to memorize p patterns, $\vec{\xi}^\mu$ with $\mu = 1, 2, 3, \ldots, p$ instead of just a single pattern, then the learning rule is modified, namely

$$J_{ij} = \epsilon \sum_{\mu=1}^{p} \xi_i^\mu \xi_j^\mu. \qquad (31)$$

Here, we start with an empty memory, i.e. initially $J_{ij} = 0 \, \forall i, j$. After fixing the strength of the pairwise J-coupling in this way, the patterns are 'memorized' by the NN, and, when presented with some initial state, the NN will evolve towards a minimum of H_H associated with one of these patterns. The

---

[5] In this brief account, we consider the system at zero temperature only.

upper limit for the number of patterns that such a network may faithfully recall via its associative memory is about $0.14N$ (Rojas 1996).

Now, it will be discussed how a linear Coulomb crystal of trapped ions may be employed to realize a Hopfield-type NN. We have already noted the similarity between H_H (equation (29)) on one hand and the two spin Hamiltonians $H_s^{(a)}$ (equation (3)) and $H_s^{(ion)}$ (equation (19)) for $J_{ij}^{(x)} = 0 = J_{ij}^{(y)}$ on the other. A further similarity can be seen between equation (31), defining the synaptic strengths in the Hopfield model, and equation (16), where the ion spin coupling constants are given. We rewrite equation (16) using expression (17) assuming a constant field gradient and obtain

$$J_{ij}^{(ion)} = \frac{\hbar}{2m} \partial_z \omega \sum_{n=1}^{N} \frac{1}{v_n^2} S_{in} S_{jn}, \qquad (32)$$

where the matrix elements S_{in} may assume positive and negative values, however usually different from ± 1 as in the generic Hopfield model. Also, the sum in equation (32) extends over all N vibrational modes instead of p patterns, and the contribution to $J_{ij}^{(ion)}$ from each vibrational mode n is weighted by the square of the respective vibrational frequency v_n. Despite these differences, it is possible to store spin patterns with trapped ions in a robust way.

What are the patterns, based on the learning rule (32), that can be stored by a trapped ion neural network? The orientation of a specific ionic spin i in a pattern $\vec{\xi}$ of spin orientations is determined by the sign of S_{in} for a given vibrational mode n. In the case of the COM mode, for example, we have $S_{in} > 0$ (or $S_{in} < 0$) $\forall i$ which means that in the two associated patterns all spins are either pointing up or all down.

Numerical simulations (Pons *et al* 2007, Braungardt *et al* 2007) show that in order to robustly store a pattern of spin orientations, it is necessary to adjust the trapping potential such that the vibrational frequencies v_1 and v_2 (that appear in the learning rule (32)) are nearly degenerate. This can be achieved by using ion traps with segmented electrodes where the Hessian of the trapping potential can be tuned by applying suitable voltages to individual segments (Hugh and Twamley 2005, Wunderlich and Wunderlich 2009). The robustness of the ion NN has been quantified by Monte Carlo simulations for a string of 40 ^{40}Ca$^+$ ions trapped such that the two lowest vibrational modes characterized by v_1 and v_2 are nearly degenerate. For this purpose, a spin pattern $\vec{\xi}^\mu$, $\mu = 1, 2$, corresponding to either one of the two modes is prepared as the initial condition of the ions' spin orientations. Then a fixed number r of spins are randomly selected and their state is inverted. This is followed by the time evolution of the ion string until an equilibrium state is reached. The probability of the ion string ending up in the initial pattern is found to be more than 97% even when up to eight randomly selected spins are initially in the wrong state (i.e. they do not match the desired pattern). Thus, even with 20% of the spins being flipped, the ion string returns towards a desired pattern.

So far we have looked at the robustness of a Hopfield-type neural network where each node consists of a single ion and which is used for classical information storage. For a *quantum* neural network, the elementary unit for information

processing is, instead of a single spin-1/2 with two eigenstates corresponding to $|0\rangle$ and $|1\rangle$, a pattern $\vec{\xi}$ of N spins. In Pons *et al* (2007) and Braungardt *et al* (2007), it is detailed how an appropriately chosen set of patterns with eight trapped ions may be used as qubits thus forming a quantum neural network. In particular, single-qubit gates and two-qubit gates by adiabatic passage are worked out that make use of additional effective fields.

2.4. Mesoscopic systems

The question if and to what extent quantum mechanical effects play a role in mesoscopic or even macroscopic systems was already posed shortly after quantum theory was developed (Schrödinger 1935). Except concerning some particular physical phenomena, for example macroscopic currents in a superconducting material, it is usually assumed that superposition states, interference and entanglement are not relevant when dealing with entities made up from a large number of individual constituents that, in addition, may interact with a noisy environment at non-zero temperature, for example biologically relevant molecules. Indications that quantum mechanics indeed plays an important role even for large molecules come from recent experiments where interference with C_{70} molecules was observed (Hackermuller *et al* 2004).

A theoretical study of how dephasing caused by coupling to a noisy environment can actually assist in transferring energy (or information), instead of impeding it, across a network of quantum nodes is presented in Plenio and Huelga (2008). It is shown that in a simplified model, light-harvesting molecules may take advantage of this process. An experimental verification directly with these molecules is difficult at present. However, trapped ions may be used to implement a suitable model to test such a prediction. For a first simple demonstration, appropriately chosen internal levels of a single ion may be used to model the nodes of a network and induced and spontaneous transitions between these levels to mimic energy transport.

Another recent theoretical study demonstrates that entanglement may persist in a model two-spin molecule even when it is exposed to a decohering hot environment, a situation typically encountered for biological molecules (Cai *et al* 2008). The time-dependent Hamiltonian modelling the two-spin molecule used for this study is

$$H_M(t) = J(t)\sigma_x^1 \sigma_x^2 + B(t)\left(\sigma_z^1 + \sigma_z^2\right). \qquad (33)$$

This molecule is then coupled to a noisy environment modelled by a master equation. After performing a unitary transformation such that $\sigma_x \to \sigma_z$ and $\sigma_z \to -\sigma_x$, we recognize a time-dependent variant of the quantum transverse Ising model (4) which could be realized with an ion spin molecule by using the spin coupling present in equation (16) and by adding a driving field as in equation (22).

3. Quantum optics simulating quantum optics

The formal similarities for creation and annihilation operators for photons and phonons on one hand and spin $S = 1/2$

particles on the other hand suggest the equivalence of various and seemingly different experiments within the field of quantum optics. In this notion, a Ramsey measurement might be regarded as simulating a Mach–Zehnder interferometer, since a wavefunction is coherently split and recombined after independent time evolution of its constituents. Therefore, one general proposition which also holds for other classes of experiments discussed in this paper may be of particular importance here: simulation goes both ways. If the Hamiltonian describing a set-up in an ion trap, possibly including static and radiation fields, is equivalent to the Hamiltonian of another system, then the ion-trap experiment can be thought of as a simulation of the other system of interest. But on the other hand, it also means that this other system might reveal some insights into certain aspects and experiments in ion traps and, depending on the specific technical difficulties when trying to perform it in an ion trap, it might also be imaginable to simulate some aspects of ion-trap physics in other systems. As pointed out earlier, however, trapped laser-cooled ions are a flexible, well-controlled and well-understood system, which can be brought into a variety of regimes, where the physics resembles other systems. Nowadays we are familiar with the fact that photons as well as the internal states of particles can be entangled (or combinations of photons and internal states), and it might sound unusual to phrase any such experiment as a simulation of another. Nevertheless, the creation and detection of entanglement of particles or photons is subject to different problems and certain aspects of entanglement and its meaning in investigating fundamental questions of quantum mechanics might best be looked at in either approach (Wineland *et al* 1998).

3.1. Theoretical background

In the early days of quantum information, it already became clear that quantum computing at a level of factorizing large numbers would be a *daunting task* (see Wineland *et al* (1998)), though, since then, astonishing progress has been made in this field. The first articles considering quantum simulations were, to some extent, motivated by the insight that the requirements for quantum simulations (in terms of gate fidelity, etc) are less stringent despite their potential to investigate systems that are beyond the reach of simulations with classical computers. Despite all progress, this statement still holds and is one motivation for this paper.

The experiments in quantum optics that are considered in Wineland *et al* (1998) and Leibfried *et al* (1997) can be simulated by trapped ions interacting with radiation fields that drive Raman transitions between hyperfine levels. A similar description can be obtained when these transitions are directly driven using microwaves (using auxiliary inhomogeneous magnetic fields) (Mintert and Wunderlich 2001, 2003, Wunderlich 2002, Johanning *et al* 2009) or when optical transitions between metastable states are used. For a harmonically bound atom interacting with two travelling wave light fields, both detuned from any real state and with frequency difference $\Delta\omega$ and phase difference ϕ, the Hamiltonian in the interaction picture can be brought

into a form $H_{\epsilon l}$ (after rotating wave approximation and adiabatic elimination of the near-resonant excited states and in the Lamb–Dicke limit $\eta^2 \langle (a + a^\dagger) \rangle \ll 1$) (Wineland *et al* 1998) with integer l indicating changes in the motional state and $\epsilon \in [0, 1]$ indicating changes in the internal state. These Hamiltonians are frequently used in experiments with laser-cooled ions; to name a few, H_{10} is called the carrier transition, H_{12} is the second blue sideband, H_{01} is called coherent drive and H_{02} is the squeeze drive. Nesting and concatenating operators taken from the set $H_{01}, H_{02}, H_{03}, H_{10}, H_{11}, H_{12}, H_{13}$ is sufficient to efficiently generate a wide range of Hamiltonians, such as the Hamiltonian for a spin $s = 1/2$ particle with mass μ in an arbitrary potential (Leibfried *et al* 2002).

These chaining of Hamiltonians could be used for a variety of experiments, such as, just to highlight a few, the phonon maser (Wallentowitz *et al* 1996) and three-phonon down conversion (Wineland *et al* 1998), and has been used to create motional cat states (Monroe *et al* 1996b), coherent states (Meekhof *et al* 1996a, 1996b) and a Hamiltonian similar to two photon excitation in cavity QED (Leibfried *et al* 1997). An example discussed in the following subsection is an experimental analogy to a nonlinear two-beam (e.g. Mach–Zehnder) interferometer as proposed in Wineland *et al* (1998). Using ions for the implementations allows for high state preparation and detection efficiency and eliminates the need for data postselection.

All the above experiments used only a single ion, and innumerable possibilities come into reach using multiple ions. The first demonstration of the CNOT gate (Cirac and Zoller 1995) was a step in this direction using, however, a single ion and its motional degree of freedom (Monroe *et al* 1995a). This concept can be adapted to entangle different atoms when it is carried out after the state of one ion is mapped onto the centre-of-mass (CM) mode and afterwards mapped back (Schmidt-Kaler *et al* 2003, Leibfried *et al* 2003).

3.2. Experiments

As a demonstration of a quantum simulation with a single ion, the Hamiltonians H_{11}, H_{12}, H_{13} are used in Leibfried *et al* (2002) to simulate a set of two nonlinear beam splitters forming a nonlinear Mach–Zehnder interferometer. A single ^{9}Be$^+$ ion provides the internal state $|a\rangle$ with

$$|0\rangle_a = |F = 1, m_F = -1\rangle$$
$$|1\rangle_a = |F = 2, m_F = -2\rangle \tag{34}$$

and the motional state $|n\rangle_b$ labelling the nth vibrational state. The experimental sequence is depicted in figure 6 and is as follows: the ion is cooled to the ground state of motion $|1\rangle_a |0\rangle_b$. A Raman $\pi/2$ pulse applied to the appropriate sideband is used to create a state proportional to $|1\rangle_{a'} |0\rangle_{b'} + |0\rangle_{a'} |n\rangle_{b'}$. This is equivalent to a beamsplitter: analogous to coherently splitting light into two separate directions, the population is coherently split into two states which, in this case, differ in both internal and motional quantum numbers. Subsequently the potential of the endcap electrodes is changed yielding trap frequency change $\Delta\nu_{z,1}$ for a time t which
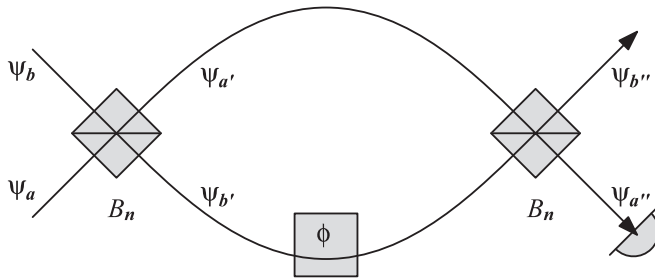
Figure 6. Ion-trap Mach–Zehnder interferometer: the manipulation of the wavefunction of a trapped ion can be thought of as analogous to a set of two nonlinear beamsplitters forming a nonlinear Mach–Zehnder interferometer.

introduces a phase shift $n\Delta\nu_{z,1}t = n\phi$ when the ion is in the nth vibrational level. Finally, a second $\pi/2$ pulse on the same sideband is applied which maps the phase difference to the population in the internal states $|0\rangle_a$ and $|1\rangle_a$ which is measured by Doppler cooling and fluorescence detection. The absolute acquired phases are irrelevant as is the total arm length of a Mach–Zehnder interferometer: longer arms only tend to make it more susceptible to perturbations; however, the signal at the outputs is given by the differential phase shift. The sequence is repeated to improve the signal to noise ratio and to extract the sinusoidal time evolution in the different states.

The experiment can be interpreted as a nonlinear Mach–Zehnder interferometer. A nonlinear beamsplitter can annihilate a photon in mode a while creating n photons in mode b (or vice versa). The annihilation operator a is replaced in this experiment by the atomic raising operator σ^+ between the states $|F = 2, m_F = -2\rangle$ and $|F = 1, m_F = -1\rangle$. These two operators are not equivalent but they act the same as long as the $\{|0\rangle_a, |1\rangle_a\}$ subspace is not left, which is fulfilled as long as the input state is $|1\rangle_a |0\rangle_b$. The optical mode with lowering operator b is replaced by the motion along a selected direction and phonon number states $|n\rangle_b$. A nth-order nonlinear beamsplitter is then given as

$$B_n = \hbar\Omega_n[a(b^\dagger)^n + a^\dagger(b)^n]. \tag{35}$$

When this operator brackets an operator that causes a phase shift in one arm by $n\phi$, the system resembles a Mach–Zehnder interferometer and the probability of detecting a phonon in output a'' becomes

$$P_{a''} = \tfrac{1}{2}[1 - \cos(n\phi)]. \tag{36}$$

This experiment requires a sideband transition in the nth sideband, which can be very inefficient with increasing n as the sideband Rabi frequencies scale with η^n and the preparation becomes slow. A faster alternative route exploiting an auxiliary state and first-order sidebands is detailed in Wineland *et al* (1998).

An increase in fringe frequency proportional to the order of the nonlinearity is found but the fringe contrast is reduced with increasing n, as preparation and manipulation imperfections spoil the fidelity of the states and the detection efficiency is below 1 for all experiments. The sensitivity of the output signal to phase changes is maximized at the steepest slope of the signal and the signal to noise ratio for the $n = 2$ and $n = 3$ measurements is found to exceed that of a perfect

first-order interferometer with unit detection efficiency. A potential improvement by increasing n from 2 to 3 is almost perfectly cancelled by the reduction of fringe contrast in the data presented in Leibfried *et al* (2002).
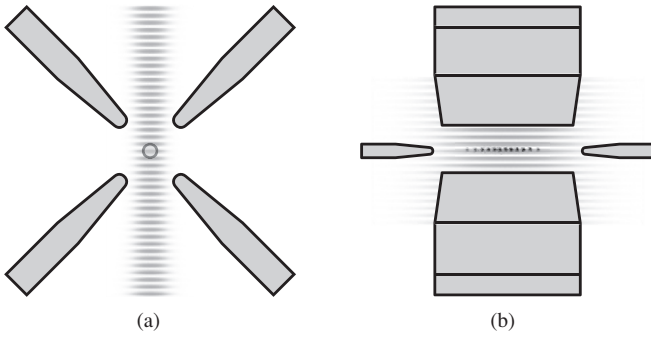
4. Transverse standing wave: Bose–Hubbard physics (and beyond)

Laser cooling and trapping have been considered (Hänsch and Schawlow 1975, Wineland and Dehmelt 1975) and successfully applied (see Ghosh (1995), Metcalf and van der Straten (2001), and references therein) to both neutral atoms and ions. Both types of laser cooling experiments are often very much alike not only in terms of the description of the experiment (trap frequencies and depths, Rabi frequencies, etc) but also in terms of experimental techniques. A recent topic in cold neutral atom physics is the combination of cold trapped atoms and optical lattices which allows us to experimentally investigate the Bose–Hubbard model (Fisher *et al* 1989), which is related to the Hubbard model in solid-state physics (Hubbard 1963). The freedom in changing tunnelling and interaction parameters, the defect-free optical lattices and the controlled introduction of disorder (Schulte *et al* 2006) allow nice and clean experiments (Greiner *et al* 2002, Morsch and Oberthaler 2006). Also, fermionic atoms have been loaded into traps and lattices and brought to quantum degeneracy. The description of such experiments by the Bardeen–Cooper–Schrieffer (BCS) theory (Bardeen *et al* 1957, Giorgini *et al* 2008) is known from superconductivity, and this analogy encourages the hope that these experiments can help to investigate and understand high T_c superconductivity (Hofstetter *et al* 2002, Holland *et al* 2001).

The large and long-range Coulomb force being the dominant force in ion traps has a number of consequences: trap frequencies, trap depths, interaction energies and particle separations are typically higher by orders of magnitude compared to traps for neutral atoms. Thus Bose–Einstein condensation (and also Bose–Hubbard physics), one long sought holy grail in quantum optics, has therefore been investigated with neutral atoms but not with ions; when cooling neutral atoms at sufficient density, their wavefunctions can overlap and a macroscopic population of the trap ground state forms (Anderson *et al* 1995, Davis *et al* 1995a). When on the other hand an ion chain is cooled to the lowest vibrational mode (Diedrich *et al* 1989), the ion separation is orders of magnitude larger than the spatial extension of the wavefunction.

But quantum degeneracy and Bose–Hubbard physics can still be simulated in ion traps when the ions take the role of lattice sites which can be populated by phonons, more specifically excitations of the vibrational modes transverse to the weak trap axis. The phonons therefore represent the neutral atoms located in one lattice site and phonons can tunnel between sites as do the atoms in optical lattices. Furthermore, as we will see later on, the phonons can be made interactive by anharmonicities in trapping potential. These anharmonicities can be introduced by the light shift of an off-resonant standing wave (see figure 7). This could be used to demonstrate a Bose–Einstein condensate (BEC)

Figure 7. Experimental set-up (not to scale) for the simulation of Bose–Hubbard physics. Images (a) and (b) are sketches of the trap and the applied standing wave potential, respectively. The illustrations are not drawn to scale; especially the wavelength of the standing wave is greatly exaggerated for visual clarity. (a) The trap as seen from one of the endcap electrodes. (b) The set-up from the side, as seen in most cases from an imaging detector; the weak trap axis is perpendicular to the standing wave.

of phonons (Porras and Cirac 2004b), the superfluid–Mott-insulator transition (Deng *et al* 2008) and, at higher levels of interaction energy, the Tonks–Girardeau gas (Deng *et al* 2008) and even frustrated XY models (Schmied *et al* 2008). In 1D, the BEC at non-zero temperature is only possible when the number of atoms (or here phonons) is finite, and we are in the weak coupling regime, which means that the average interaction energy is smaller than the expectation value of the kinetic energy. A peculiarity of the effective phonon interaction being dependent on the position of the standing wave is that it can be tuned, even in sign, similar as the magnetic field can change the scattering length near a Feshbach resonance.

Besides the general appeal to demonstrate Bose–Einstein condensation in yet another system, Bose–Hubbard physics in ion traps offers advantages, and also drawbacks, over present neutral atom experiments: experiments in ion traps do not only offer global control of the tunnelling rate and interaction energy (as we will see later), equivalent to ramping the optical lattice depth or applying a magnetic field to obtain a certain scattering length near a Feshbach resonance. Ion traps also allow for local control: irregular lattices correspond to site-dependent tunnelling rates and can be obtained in segmented microtraps; the interaction energy can as well be made site dependent by having independent standing wave intensities and phases at the different ion positions—in terms of neutral atoms, this would correspond to arbitrary 3D Feshbach magnetic fields. Other interesting features include single site control and readout of the state and the potential to extract the density matrix either partially or even fully (in small systems). On the other hand, the experiments discussed here are restricted to bosonic phonons and thus Bose–Hubbard physics and today's ion traps are mostly restricted to one dimension but true two-dimensional systems can be obtained in surface traps (Seidelin *et al* 2006).

4.1. Background

When we speak of phonons in the context of linear ion traps, we often think in terms of axial normal modes. In this

situation, momentum is transferred by local interaction with the addressed ion which couples efficiently to the motion of the whole chain due to changing separations and acting Coulomb forces. In this section, radial modes of the ion motion are considered. Classically, a radial displacement of a single ion excites both the radial motion of other chain members and the axial motion of the whole chain. But when the axial ion separations are much larger than the radial excursion of the ion motion, the coupling of this motion to all other modes is very inefficient: the motion is almost perfectly perpendicular to the Coulomb interaction between ions all the time and does not change the ion separations to first order. Thus, radial phonons can be viewed as being located to one ion but the non-vanishing coupling makes the localization non-permanent and re-emerges as a finite phonon tunnelling rate.

The Hamiltonian describing the system reads as (Deng *et al* 2008)

$$H_0 = \sum_{i=1}^{N} \frac{p_i^2}{2m} + V_T + \sum_{i,j=1,i>j}^{N} \frac{1}{4\pi\epsilon_0} \frac{e^2}{|\vec{R}_i - \vec{R}_j|}, \quad (37)$$

where the trapping potential V_T could be simply quadratic like the effective potential created by a simple linear Paul trap or be an array of microtraps achieved by micro-structuring (Rowe *et al* 2002, Stick *et al* 2006). We will look in more detail into one radial coordinate x and excitations at the trap frequency $\nu_{x,1}$ in this direction. The trap frequency $\nu_{y,1}$ can be chosen to be non-degenerate to allow for addressing specific sidebands and to avoid unwanted couplings. The absolute value of the Coulomb force between two particles separated by a large distance δz in the z-direction and displaced only slightly by δx in the x-direction is

$$|\vec{F}| = \frac{e^2}{4\pi\epsilon_0} \frac{1}{\delta x^2 + \delta z^2} \approx \frac{e^2}{4\pi\epsilon_0} \frac{1}{|\delta z|^2}. \quad (38)$$

The component in the x-direction of the Coulomb force is given by

$$F_x = |\vec{F}| \frac{\delta x}{\sqrt{\delta x^2 + \delta z^2}} \approx |\vec{F}| \frac{\delta x}{|\delta z|}. \quad (39)$$

When the radial separation δx is identified with $x_i - x_j$ and the axial separation δz with the unperturbed $z_i^0 - z_j^0$, the radial potential for small relative displacements becomes

$$H_{\text{Coulomb},x} \approx -\frac{1}{2} \frac{e^2}{4\pi\epsilon_0} \sum_{i,j=1,i>j}^{N} \frac{(x_i - x_j)^2}{|z_i^0 - z_j^0|^3}. \quad (40)$$

Introducing the quantities

$$t_{i,j} = \frac{1}{2} \frac{1}{4\pi\epsilon_0} \frac{e^2}{m\nu_{x,1}^2} \frac{\hbar\nu_{x,1}}{|z_i^0 - z_j^0|^3}$$

$$\nu_{x,1}^{(i)} = \nu_{x,1} - \sum_{j=1,j\neq i}^{N} t_{i,j}, \quad (41)$$

the second quantized form becomes (Deng *et al* 2008)

$$\frac{H_{x0}}{\hbar} = \sum_{i=1}^{N} \nu_{x,1}^{(i)} n_i + \sum_{i,j=1,i>j}^{N} t_{i,j} \left(a_i^\dagger + a_i\right)\left(a_j^\dagger + a_j\right). \quad (42)$$

The quantities $t_{i,j}$ are site-dependent hopping terms resulting from the non-vanishing coupling of the radial motion between

J. Phys. B: At. Mol. Opt. Phys. **42** (2009) 154009

Review

all ions in the chain. The closer the ions, the stronger the coupling of ion motions and therefore tunnelling of transverse phonons. The next-neighbour tunnelling is therefore the strongest but its slowly decaying behaviour with lattice site difference can already be seen from equation (40), leading to long-range tunnelling in stark contrast to pure next-neighbour tunnelling, as found in neutral atom experiments. The Coulomb repulsion from adjacent ions has a maximum for $\delta x = 0$ and counteracts the radial trapping potential, and $v_{x,1}^{(i)}$ are the reduced radial trapping frequencies. These changes in the radial trapping frequencies and therefore the reductions in the phonon energies are the strongest for small ion separations and thus lead to an axial phonon confinement towards the centre of the trap (Deng *et al* 2008). The more inhomogeneous the ion separations, the stronger the confinement becomes. Therefore, this effect is more pronounced in a linear ion trap compared to the isospaced array of microtraps (with almost constant ion separations) and becomes more evident with increasing ion number. Due to the large separation of ions and the small transverse oscillation amplitudes, the effect of the Coulomb interaction on the radial potential is just a change in the trapping frequency. The anharmonicities, that should in principle be already present have been neglected so far. A purely harmonic trapping potential results in equally spaced oscillator levels, meaning that the energy of having two phonons located on different sites or both at the same site gives the same total energy. Interacting phonons means that the energy of having two phonons at the same site is the sum of the two single phonon energies, altered by an interaction energy, and the oscillator levels are no longer equidistant. A nifty idea to mimic this interaction is to introduce an anharmonicity to the trapping potential and thus to break the regular spacing of the trap levels. This can in principle be done by any non-harmonic potential, for example a sinusoidal potential as known from optical lattices generated by an off-resonant standing wave with wave vector k_{SW} (Deng *et al* 2008):

$$H_{SW} = F \sum_{i=1}^{N} \cos^2\left(k_{SW} x_i + \frac{\pi}{2}\delta\right), \quad (43)$$

where F is the peak ac-Stark energy shift. For small anharmonicities, the Hamiltonian $H_{x0} + H_{SW}$ can be expanded in the Lamb–Dicke parameter $\eta_{x,SW}$ with

$$\eta_{x,SW} = \sqrt{\hbar^2 k_{SW}^2 / 2m\hbar v_{x,1}} \quad (44)$$

and is sufficiently approximated when truncated after second-order terms and the Hamiltonian can be brought into the well-known form of the Bose–Hubbard model (Deng *et al* 2008, Fisher *et al* 1989):

$$H_x^{BHM} = \sum_{i,j=1,i>j}^{N} \hbar t_{i,j}\left(a_i^\dagger a_j + H.c.\right) + \sum_{i=1}^{N} \hbar\left(v_{x,1} + v_{x,1}^{(i)}\right) a_i^\dagger a_i$$
$$+ U \sum_{i=1}^{N} a_i^{\dagger 2} a_i^2. \quad (45)$$

In this approximation of small anharmonicities, the total radial phonon number is conserved and coupling to axial modes is neglected. The third term in equation (45) has a
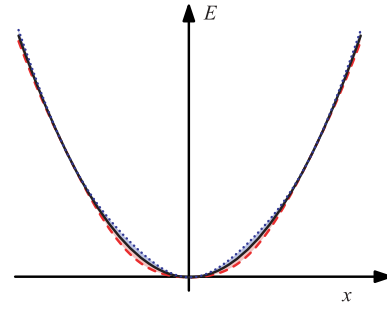
Figure 8. The transverse potential as a sum of a parabolic trapping potential plus a far off-resonant standing wave. The solid curve with medium curvature shows the unperturbed effective trap potential, while the dashed curve with lowest curvature is the total effective potential with a standing wave having an antinode at the ion position, resulting in a effective repulsive interaction of phonons. The dotted curve with highest curvature shows the total effective potential with a standing wave having a node at the ion position, resulting in a effective attractive interaction of phonons.
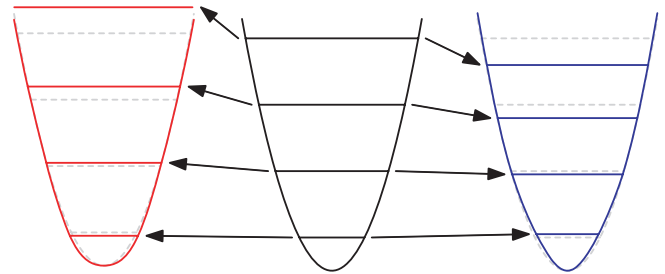
Figure 9. Shifts of the harmonic oscillator levels due to the standing wave (not to scale). The centre image shows an undistorted harmonic trap with equally spaced energy levels. When a standing wave along x is added, such that it has an antinode at the trap centre (left-hand side), the base level is lowered due to the quadratic part in the standing wave. In addition, the higher levels are raised due to the quartic part of the dipole potential. The spacing of the levels is no longer equidistant and mimics a repulsive interaction of the phonons. For an additional standing wave with a node at the trap centre (right-hand side), the lowest level is raised due to the upward curvature of the dipole potential. The level spacing is reduced and also non-equal and pretends a attractive interaction of the phonons. The grey dashed lines in the outer graphs again indicate unperturbed potential and energy levels.

contribution proportional to the phonon number squared which is responsible for the interaction. Its strength is scaled by (Deng *et al* 2008):

$$U = 2(-1)^\delta F \eta_{x,SW}^2. \quad (46)$$

The interaction depends on the strength and the relative position δ of the standing wave and can even change its sign (see equations (43) and (46)); it is maximal positive/repulsive for ions at the antinodes of the standing wave ($\delta = 0$) and maximal negative/attractive for ions at the nodes of the standing wave ($\delta = 1$). This can be seen in figures 8 and 9: the small sinusoidal alteration from the standing wave makes the tip of the parabola slightly pointier for a node of the standing wave or chamfered for an antinode of the standing wave which results in a shift of the trapping frequency. The interesting consequence, however, is the

differential shifts of the oscillator levels which are depicted in figure 9; the fourth-order contribution from the extremum of the sinusoidal potential has always the opposite sign of the quadratic contribution. Thus it is curved upwards for an antinode of the standing wave (meaning that the quadratic term is curved downwards) and shifts higher levels up, mimicking a repulsive interaction. A node of the standing wave has an upwards curved quadratic contribution; the fourth order is curved downwards, making the trap softer when walking away from the centre and reduces the energy of higher trap levels imitating an attractive interaction.

The Bose–Hubbard model is well known in neutral atom physics (Fisher *et al* 1989). When the total phonon number N_{ph} is an integer multiple of the ion number N_{ion}, the model predicts a transition from the superfluid state (dominated by tunnelling) to a Mott-insulator state (negligible tunnelling) with a constant phonon number per lattice site. This transition can be traversed by changing the ratio of the tunnelling frequency to repulsive interaction energy (that is, changing the trap frequency or standing wave intensity). For incommensurate phonon numbers that are not integer multiples of the ion number, a finite number of stages with constant phonon occupation can be anticipated, with the highest phonon populations at the bottom of the phonon confining potential, that is, at the trap centre. In neutral atom physics, the superfluid–Mott-insulator transition has been observed in beautiful experiments (Greiner *et al* 2002).

The framework of the Luttinger liquid theory (Luttinger 1963, Voit 1995) predicts algebraic decay of correlations between the number of phonons for the superfluid phase when phonon tunnelling beyond next neighbours is neglected (Deng *et al* 2008):

$$C_{i,j}^{nn} = \langle n_i n_j \rangle - \langle n_i \rangle \langle n_j \rangle \propto |i - j|^{-2} \qquad (47)$$

and correlations that are nondiagonal in the phonon number decay as

$$C_{i,j}^{aa} = \frac{\langle a_i^\dagger a_j \rangle}{\sqrt{\langle n_i \rangle \langle n_j \rangle}} \propto |i - j|^{-\alpha} \qquad (48)$$

with $\alpha \propto \sqrt{U/t n_0}$ given by the ratio of tunnelling to interaction at the central phonon density n_0. In the Mott phase, however, both correlations decay exponentially with distance:

$$C_{i,j}^{aa,nn} \propto e^{-|i-j|/\xi} \qquad (49)$$

with the correlation length ξ.

Phonon densities and fluctuations from numerical calculation using the density matrix renormalization group method (DMRG) (White 1993) were presented in Deng *et al* (2008) for linear traps and an array of microtraps. The calculations reproduced the superfluid–Mott-insulator transition starting from the sides of the chain (due to larger ion separations, the tunnelling rate is lower at the ends). Especially for an array of microtraps, the Mott phase features an almost flat mean phonon number per lattice site along the chain for a commensurate ion and phonon number and the fluctuations are also flat and strongly reduced. For linear traps, the inhomogeneous ion separations modulate phonon numbers and fluctuations which are both more peaked at the

chain centre. The correlations in the superfluid phase are found to be in agreement with equations (47) and (48) for short (linear trap) and intermediate (microtrap array) distances, and signatures of finite size effects and inhomogeneous ion separations can be seen and are found to be more important in linear traps. In addition, long-range correlations in the Mott phase are found that can be attributed to the long-range hopping terms in equation (41). For large repulsive interactions and incommensurate filling the system was found in Deng *et al* (2008) to form a Tonks–Girardeau gas (Girardeau 1960, Lieb and Liniger 1963) which has been recently observed in neutral atoms (Paredes *et al* 2004, Tolra *et al* 2004). Due to their repulsion, the phonons cannot get past each other and attain the hard core bosons limit and tunnelling is suppressed. The atoms/phonons behave neither purely bosonic nor fermionic, because they can occupy the same momentum state but not the same position in space. Mathematically, there is an exact one-to-one mapping between impenetrable bosons and non-interacting fermions for a one-dimensional system. Numerical studies in Deng *et al* (2008) for an array of microtraps and half-filling ($N_{ph} = 1/2 N_{ion}$) show a constant phonon number distribution together with algebraically decaying correlations. The exponent of the decay deviates from the value $1/2$ which is expected for a Tonks gas with nearest-neighbour interaction only. This is explained by mapping the BHM to a XY model with antiferromagnetic dipolar interactions. Deng *et al* (2008) also studied attractive systems and used site-dependent interactions to construct systems with highly degenerate ground states described by an XY model.

4.2. Experiments

For a string of 50 ions with a minimum axial separation of 5 μm and a radial trapping frequency $\nu_{x,1}$ about 70 times higher than the axial trapping frequency $\nu_{z,1}$, the tunnelling rates t_{ij} were found to be comparable to the axial trapping frequency. For $F = \hbar \nu_{x,1}$ which is realistic with commercially available laser systems, the axial frequency is changed by a few 10% and the system remains in the phonon number conserving regime and the phonon interaction energy U is approximately twice the tunnelling rate (Deng *et al* 2008).

The interesting quantities are the number of atoms at each lattice site, corresponding to the number of transverse phonons at each ion, their fluctuations and their correlations. Phonon occupation cannot be measured directly but can be mapped on the internal state and the ions' resonance fluorescence is recorded. The mapping is accomplished by sideband transitions with carrier Rabi frequency Ω—note that a sideband does not refer to the axial mode as usual but to the radial mode along the x-axis here. Since the strength of the sideband transition depends on the expectation value of the phonon number, the transition matrix element and therefore the vibrational state can be extracted from repetitive measurements (Meekhof *et al* 1996a, 1996b, Leibfried *et al* 1996). If the ion is not in a Fock state, each phonon population contributes to a $\sin^2(\sqrt{n} \Omega t)$ term in the temporal evolution, which is accordingly given by

$$P_\uparrow = \sum_n P(n) \sin^2(\sqrt{n} \Omega t) \qquad (50)$$

with $P(n)$ being the probability of having n phonons. Different frequency components in the temporal evolution can be extracted from Fourier analysis to yield P_n (Meekhof *et al* 1996a, 1996b, Leibfried *et al* 1996) and reveal directly a transition from superfluid to the Mott-insulator state. For a Mott insulator, all ions are in the same vibrational state and therefore have the same transition matrix element (assuming the number of phonons being an integer multiple of the ion number). Exciting sideband transitions on all ions simultaneously brings all of them into the same internal state, so for appropriately chosen (π-pulse) times the whole chain will switch from dark to bright. For a superfluid, however, the phonon expectation value is not a constant along the chain, and there is no universal π-pulse and the ions will never undergo common oscillations from the dark to the bright state when varying the interaction time. If desired, the whole density matrix can be deduced from quantum state tomography which, of course, becomes tedious or, for all practical purposes, even impossible for long chains.

4.2.1. Superfluid–Mott-insulator transition and creation of a superfluid phonon state by adiabatic evolution. This experiment is similar to the superfluid–Mott-insulator transition by Greiner *et al* (2002) obtained by ramping the optical lattice depth. A clear demonstration, as proposed in Porras and Cirac (2004b), would start with an ion chain cooled to a state with zero radial phonons, the 'radial ground state'. The optical lattice is ramped up to a high intensity $U \gg t_{ij}$ such that the ions sit on a node of the standing wave and the phonons experience a repulsive interaction. A defined number of phonons is introduced by sideband transitions, such that the total phonon number is an integer multiple of the ion number (e.g. by a π pulse on the blue sideband). If now the phonon number is mapped back to the internal state by sideband transitions, a collective switching from the internal bright to the non-scattering state should be observed, that is, the time for a π pulse is identical throughout the whole chain. Alternatively, the interaction U is adiabatically reduced down to a final strength $U_{\rm f}$ (the standing wave intensity is lowered), such that the system remains in the ground state. At a critical value $U_{\rm f} \approx t_{ij}$, the system undergoes a transition to a phonon superfluid. When measuring phonon occupation numbers by mapping them to internal states by sideband transitions, the phonon numbers can be expected to be inhomogeneous, due to the phonon trapping potential and non-negligible tunnelling.

4.2.2. Bose–Einstein condensation by evaporative laser cooling. Evaporative laser cooling for phonons in ion traps sounds like an oxymoron because in neutral atom physics evaporative cooling terms a process free of laser scattering, where only the highest energy atoms can leave the trap (Davis *et al* 1995b) and take more than the average thermal energy with them which, provided sufficient fast thermalization, results in a cooler cloud. The analogy is that in the ion trap with an axial phonon confining potential high phonon occupations (labelled high energy phonons in Porras and Cirac (2004b)) can more easily tunnel to the ends of the chain, analogous to

hot atoms, and when laser cooling is applied to these ends exclusively, the phonons are removed or evaporated.

A demonstration would start with a Doppler-cooled ion chain with a given number of phonons per site. Applying laser cooling at the ends of the ion chain removes or evaporates high energy phonons (or phonon occupation numbers) from the top of the phonon confining potential. A small interaction $U \ll t_{ij}$ allows for a phonon–phonon interaction and therefore for thermalization, equivalent to the need of a non-vanishing scattering length for thermalization of neutral atom clouds and finally Bose–Einstein condensation of phonons can be observed. Since this is a 1D system, the BEC cannot take place in the thermodynamic limit $N \rightarrow \infty$ at finite temperature, but for a given number there will be a non-zero transition temperature. In contrast to the Mott insulator (phonon Fock state), the signature of this phase transition is more difficult to extract. One can deduce phonon occupation distribution from series of fluorescence images after sideband transitions of varying time. Evaporative laser cooling for phonons should reveal an abrupt transition from a thermal phonon occupation distribution to the BEC distribution, which corresponds to a distinction of a Gaussian and a Thomas–Fermi momentum distribution for neutral atoms.

It could be interesting to modify the axial trapping potential in microtraps such that the equilibrium positions are really equidistant and the phonon trapping potential becomes flat, corresponding to unconfined phonons and a demonstration Bose–Einstein condensation of free particles, similar to experiments by Meyrath *et al* (2005).

4.3. Frustrated XY models

For large anharmonicities, strong repulsion and low filling factor $N_{\rm ph} \ll N_{\rm ion}$, the occupation by two phonons becomes unlikely and the system attains the hardcore boson limit. The phonons can be mapped to $S = \frac{1}{2}$ spins via the Holstein–Primakoff transformation as $a_\alpha^\dagger \rightarrow S_\alpha^+$, $a_\alpha \rightarrow S_\alpha^-$ and $n_\alpha \rightarrow S_\alpha^z + \frac{1}{2}$. The resulting Hamiltonian is an XY model with dipolar interactions and a site-dependent potential (Schmied *et al* 2008):

$$H_{\rm S} = 2 \sum_{\langle \alpha, \beta \rangle} t_{\alpha,\beta} \left(S_\alpha^x S_\beta^x + S_\alpha^y S_\beta^y \right) + \sum_\alpha V_\alpha S_\alpha^z. \qquad (51)$$

Hamiltonians like these are interesting because they allow us to investigate frustrated XY models in one and two dimensions. Frustration is a phenomenon relevant in condensed matter physics and describes the situation where, due to the lattice geometry or competing interactions, the interaction energies cannot be simultaneously minimized which can result in highly non-degenerate ground states with non-zero entropy, even at zero temperature. Such frustrated XY models can now be investigated in 1D and 2D systems, that is, in linear chains and planar zigzag structures in linear ion traps and planar structures in surface traps.

The 1D case leads to the $S = \frac{1}{2}$ XY antiferromagnet with dipolar interactions, which becomes exactly solvable if only next-neighbour interactions are considered. By weakening the transverse confinement along one direction, the linear chain is no longer the energetically favoured pattern and the ions

J. Phys. B: At. Mol. Opt. Phys. **42** (2009) 154009

Review

arrange themselves in a planar zigzag ladder which can be viewed as two linear chains relatively displaced to each other. By variation of the radial trapping potential, the properties of this two-dimensional structure, namely the zigzag amplitude and thus the ratio of the dominant inter-chain (t_1) to intra-chain (t_2) coupling, can be tuned. The zigzag amplitude ξ, measured in units of the inter-ion spacing, is limited by the fact that for too weak a transverse confinement the ion chain spontaneously flips into helical order (around $\xi \approx 0.965$). This in turn limits the accessible range of coupling ratios when phonons perpendicular to the zigzag plane are considered. But when we exploit the phonons in the ladder plane, any $|t_2/t_1| > 1/8$ ratio can be accessed. For low zigzag amplitudes and intra-chain couplings, the ladder is found to exhibit a long-range antiferromagnetic Néel order and undergoes a transition at $\xi \approx 0.461$ to spiral order which shows both spontaneous magnetic order and chiral order.

The chirality can be defined as

$$\kappa_i = 4\left(S_i^x S_{i+1}^y - S_i^y S_{i+1}^x\right), \tag{52}$$

and the chiral order parameter is the averaged chiral correlation over all ion pairs in the ladder:

$$O_\kappa^\Delta = \frac{1}{L-1-|\Delta|} \sum_i \langle \kappa_i \kappa_{i+\Delta} \rangle$$

$$O_\kappa = \frac{1}{2L-3} \sum_{\Delta=-(L-2)}^{L-2} O_\kappa^\Delta. \tag{53}$$

When we envision an experiment measuring this chiral order, we first have to remember that the spins in (52) are not real spins but phonons mapped back via the Holstein–Primakoff transformation and that the probability of having double phonon occupation is negligible. The expectation values for the phonon occupation are thus given by the probability of having single phonon occupation. To measure chirality and the chiral order parameter, we have to measure phonons in both transverse modes for each ion and their correlations by sideband transitions. When the measurement is repeated for different radial confinements and thus coupling ratios, the transition from Néel to spiral order can be observed. Another interesting feature to look at is a yet-not-understood 'reorientation transition' around $\xi \approx 0.8$ found in numerical calculations of up to 20 ions (Schmied *et al* 2008) which gets more pronounced for larger ion numbers. Furthermore, the convergence of the numerical algorithm used in Schmied *et al* (2008) shows poor convergence for equal inter- and intra-chain couplings and thus a measurement of the phonon correlation function in this regime could be interesting.

Even more variations are possible in extended planar lattices, for example triangular lattices as considered in Schmied *et al* (2008). Rotating planar triangular Wigner crystals have been observed in Penning traps (Mitchell *et al* 1998) and again they can be viewed as displaced linear chains such that it is possible to define a ratio of inter- to intra-chain couplings. A variety of phases has been found when the orientation of the co-rotating standing wave and therefore vibrational motion is changed relative to the lattice normal (Schmied *et al* 2008). Another approach to implement such
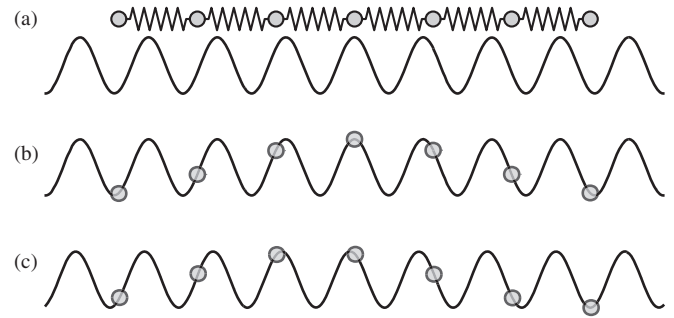
Figure 10. (a) Basic Frenkel–Kontorova model: a one-dimensional chain of atoms with next-neighbour interactions is exposed to a sinusoidal potential; (b) and (c) possible spatial configurations. The upper configuration (b) is unstable—the total energy, which is a function of the coordinates of all particles, has a saddle point, whereas configuration (c), obtained only by a minuscule sideways shift, is stable corresponding to a minimum of the total energy (after Braun and Kivshar 1998)

lattices is by means of surface traps (Chiaverini and Lybarger 2008, Seidelin *et al* 2006). The equilibrium ion positions and therefore the ratio of inter- to intra-chain couplings is given by the effective potential generated by the trap. A variation of the ratio of relevant couplings could be investigated either in a series of surface traps, each designed for an particular coupling ratio, or by electrode geometries which allow for a anisotropic deformation of the triangular lattice. It should be pointed out that such planar traps would in principle allow us to implement any desired lattice geometry.

5. Axial standing wave: the Frenkel–Kontorova ion model

The Frenkel–Kontorova model (FKM) is a model describing a linear chain of particles with harmonic next-neighbour interactions which is exposed to a sinusoidal potential (Frenkel and Kontorova 1938). The system of interest might remind the reader of the Hubbard– or Bose–Hubbard model as discussed in section 4.1; however, the Frenkel–Kontorova model is simpler, being classical and one-dimensional and, on the other hand, focuses more on classical nonlinear dynamics and chaos, and questions of integrability and the persistence of quasi-periodic motion (Braun and Kivshar 1998). Despite this simplicity, the FKM is able to describe a variety of physical phenomena such as crystal dislocations, commensurate–incommensurate phase transitions, epitaxial monolayers on a crystal surface, magnetic chains and fluxon dynamics in Josephson junctions (see Braun and Kivshar (2004), and references therein). The FKM is one of the first examples in solid-state physics where a one-dimensional chain can be used to model an extended two-dimensional defect in bulk (Braun and Kivshar 1998).

5.1. Formalism and numerical calculations

In the basic model the interactions are harmonic and restricted to next-neighbours, and the external potential is sinusoidal (see figure 10). Without this external potential, the dynamics

of the chain can be understood in terms of normal modes and is quasi-periodic. When the potential is switched on but the perturbation is small, that is, below the critical perturbation strength, the system is in the so-called sliding phase and the chain can oscillate in the lattice and the ion positions follow a Kolmogorov–Arnol'd–Moser curve (Braun and Kivshar 2004). For higher perturbations, the system undergoes an *Aubry analyticity breaking transition* (Aubry and Le Daeron 1983) and the ion chain starts to be pinned by the lattice and the positions form a devils staircase corresponding to a fractal Cantor set (García-Mata *et al* 2007). The ground state is unique for all perturbations, but in the pinned phase, a large number of states exists very close to the ground state like in a fractal spin glass (Zhirov *et al* 2002).

Various extensions and modifications of the basic Frenkel–Kontorova model have been investigated, for example arbitrary on-site potentials and anharmonic interactions between the particles (Braun and Kivshar 1998). In the following, we will focus on the Frenkel–Kontorova ion model (FKIM) which is a classical picture for a laser-cooled chain of ions trapped in a linear trap exposed to a standing wave (García-Mata *et al* 2007). For a sample of ions in a linear trap with a much stronger radial than axial confinement, the ions arrange themselves in a linear chain. When the radial motion is frozen due to laser cooling, the chain can be described in good approximation with a one-dimensional Hamiltonian. Then the interaction of the particles is given by the long-range Coulomb force and the external potential is a sum of the effective sinusoidal potential from the standing wave and the effective harmonic axial trapping potential. The Hamiltonian is given by

$$H = \sum_{i=1}^{N} \left(\frac{p_{z,i}^2}{2m} + \frac{m\nu_{z,1}^2}{2} z_i^2 - K \cos(2\pi z_i/d) \right) + \sum_{i>j} \frac{e^2}{4\pi\epsilon_0} \frac{1}{|z_i - z_j|}. \tag{54}$$

The above Hamiltonian therefore corresponds to the general ion-trap Hamiltonian given in equation (37) where only the part in the z-direction is considered and a sinusoidal potential of strength K and periodicity d is added. In García-Mata *et al* (2007), the authors investigate the dimensionless form of the above FKIM–Hamiltonian which reads as

$$H = \sum_{i=1}^{N} \left(\frac{P_i^2}{2} + \frac{\tilde{\nu}^2}{2} \tilde{z}_i^2 - \tilde{K} \cos \tilde{z}_i \right) + \sum_{i>j} \frac{1}{|\tilde{z}_i - \tilde{z}_j|}. \tag{55}$$

The ion positions $\tilde{z}$ are given in units of the reduced lattice constant $\tilde{d} = d/2\pi$ and the energy $\tilde{E}$ as well as the strength of the sinusoidal potential $\tilde{K}$ is measured in units of $e^2/4\pi\epsilon_0\tilde{d}$. The modified angular frequency is obtained as $\tilde{\nu}^2 = 4\pi\epsilon_0 m\nu_{z,1}^2 \tilde{d}^3/e^2$. In the quantum case, the momenta are given by $P_i = -i\hbar_{\text{eff}}\partial_{x_i}$ with an effective Planck constant $\hbar_{\text{eff}}$ given as

$$\hbar_{\text{eff}} = \hbar/(e\sqrt{md}), \tag{56}$$

which depends on the lattice constant which allows us to scale and investigate quantum effects as we will see later.
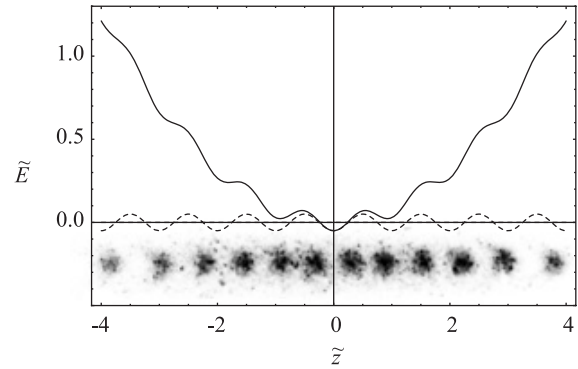
Figure 11. Frenkel–Kontorova ion model: the potential curvature, the sine ripple amplitude and lattice constant are plotted for values corresponding to the *Aubry analyticity breaking transition* at golden mean density for a chain of 12 ions with a centre separation of 5 μm. A CCD image of a string of 12 ^{172}Yb$^+$ ions is scaled to match the conditions for the potential plot and indicates the unperturbed ion positions.

First, the authors compare numerical solutions to the classical ground-state problem in the FKIM to solutions of the FKM with only next-neighbour interactions. The numerical studies are performed for up to a few hundreds of ions at the golden mean density (at the centre of the ion chain), where the average occupation of a lattice site is $(\sqrt{5} + 1)/2$ and results in the golden Kolmogorov–Arnol'd–Moser (KAM) curve for the ion positions commonly used for the studies of the Aubry transition (Aubry and Le Daeron 1983, Braun and Kivshar 2004). The FKM leads to dynamical recursive maps for the calculation of equilibrium ion positions which are found to describe the centre 1/3 part of the ion chain appropriately. By comparison of the solutions for FKM and FKIM equilibrium positions, the influence of long-range interactions and the trapping potential can be mapped out and is found to be negligible in the centre region. Here, the ion density is highest and almost constant and allows for screening of the trap potential by nearby ions, similar to the Debye radius in plasma physics. In the outer regions visible deviations in the equilibrium positions are found, as the ion density is lower at the ends of the chain.

As for the FKM, for small depths of the sinusoidal potential ($\tilde{K} < 0.05$), the chain is in a sliding phase. The hull function, which compares the unperturbed equilibrium positions to the perturbed ones modulo 2π, is continuous and the phonon mode spectrum has a sound-like form. At a critical strength of the standing wave ($K_c \approx 0.05$), as shown in figure 11, the system undergoes an *Aubry analyticity breaking transition* (Aubry and Le Daeron 1983). Above the critical lattice strength, the ion chain is in a pinned phase, their positions are described by a devils staircase, which is a fractal Cantor set (Peitgen *et al* 2004), and the phonon spectrum shows a gap. Another similarity to the FKM is that in the pinned phase, the FKIM has properties of a spin glass and features an enormous number of stable equilibrium configurations energetically close to the ground state (Zhirov *et al* 2002), despite the ground state being unique.
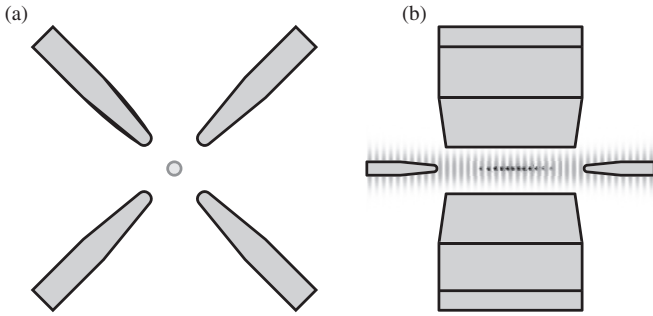
Figure 12. Schematic (not to scale) of the experimental set-up suitable for simulating Frenkel–Kontorova physics and observing an Aubry transition. The standing wave is applied in the axial direction, either by optical access through ring-shaped endcap electrodes or by crossing two beams at an angle, such that the counter-propagating component is aligned parallel to the weak trap axis. (a) The view along the ion chain and (b) the set-up as seen by an imaging detector used for measuring the ion fluorescence and for the determination of ion positions and formfactor.

So far, all considerations have been purely classical. Quantum effects were investigated in Borgonovi *et al* (1989) and the quasi-degenerate configurations close to the ground state are found to become important and tunnelling between them leads to non-trivial *instanton excitations* (García-Mata *et al* 2007). The quantum case is studied in García-Mata *et al* (2007) using the quantum Monte Carlo (QMC) approach (Grotendorst *et al* 2002, Nightingale and Umrigar 1998). To see these structural changes, the authors look at the power spectrum of the position distribution (in the classical case, z_n are the ion positions):

$$F(k) = \frac{\left\langle \left| \sum_n \exp(ikz_n(\tau)) \right|^2 \right\rangle}{\delta N}. \tag{57}$$

From these numerical solutions, a phase transition from a pinned instanton glass to a sliding phonon regime is observed, depending on the value of the *effective* Planck constant $\hbar_{\text{eff}}$ (García-Mata *et al* 2007) which can be varied by changing the lattice constant and thus the influence of tunnelling, and the transition taking place at $\hbar_{\text{eff}} \approx 1$. For low values of $\hbar_{\text{eff}}$ the formfactor shows discrete resonances which in the sliding phase are equidistantly spaced at integer multiples of the golden mean density. However, if the ions are pinned by the optical lattice, these resonances appear at integer values of k. The pinned phase also shows a quantum transition when $\hbar_{\text{eff}}$ is increased: for low values $\hbar_{\text{eff}}$, the pinned phase is not destroyed and discrete resonances are still found. For larger values of $\hbar$, the formfactor becomes continuous and the transition occurs at a value $\hbar_{\text{eff}} \approx 1$.

5.2. FKIM experiments

Experiments for investigating Frenkel–Kontorova physics require a sinusoidal potential along a one-dimensional ion chain. This can be implemented by a far off-resonant standing wave along the weak trap axis as indicated in figure 12. Being far off-resonant means that changes of the internal state due to these lasers is unlikely within the duration of the experiment. Following García-Mata *et al* (2007) the ion density at the

centre should be the golden mean density, that is, the lattice periodicity should be by a factor $(\sqrt{5} + 1)/2$ larger than the ion separation at the middle of the chain. This can be easily obtained even at a fixed wavelength by changing the angle between the intersecting beams that form the dipole potential or, alternatively, by changing the trap frequency. To obtain the golden mean density for ions separated by 5 μm, the lattice periodicity is approximately 3.1 μm corresponding for example to two beams at $\lambda = 1064$ nm, each enclosing an angle of $\alpha \approx 80°$ with the weak trap axis.

The position of the lattice has to be fixed relative to the ions which means that the relative phase of the two counter-propagating running waves has to be constant. This requires stability and potentially active feedback on mirrors. To maintain a constant depth of the sinusoidal potential along the chain, the Rayleigh range would ideally be large compared to the chain length, meaning that the waist would be large. The required strength of the standing wave K_c to observe an Aubry transition corresponding to a depth of 0.6 K ions separated by 5 μm which is much deeper than in neutral atom experiments. On the other hand the trap frequencies are much higher in ion-trap experiments and thus the timescales for a measurement are shorter, allowing for lasers which are closer to the atomic resonance, and in turn requiring less power. The challenging power requirements can be lessened when the light cycles in a resonant cavity, however, with a more demanding stability.

The effective Planck constant as given in equation (56) contains the lattice constant and can in principle be changed by adjusting either the wavelength of the light that forms the sinusoidal dipole potential or the angle between the intersecting beams. To maintain the golden mean density, the trap frequency would be varied simultaneously. For parameters given above, however, the effective Planck constant is approximately 3×10^{-5} (calculated for Ca ions (García-Mata *et al* 2007)) and due to the weak dependence on the lattice constant (see equation (56)) ion-trap experiments are likely to be restricted to the semi-classical regime with $\hbar_{\text{eff}} \ll 1$, hardly accessible for QMC calculations (García-Mata *et al* 2007).

The experiment would start with an ion chain cooled to the ground state. Ramping the standing wave along the weak trap axis adiabatically up to the desired final strength ensures that the system remains in its ground state and the equilibrium positions and thus the formfactor can be measured.

Beside the general interest in the Frenkel–Kontorova physics, an axial standing wave as discussed above might also prove to be useful in the context of quantum information with ion traps since the strong gap in the phonon spectrum found in the pinned phase might allow for the protection of quantum gates against decoherence (García-Mata *et al* 2007).

6. Quantum fields and relativistic effects

6.1. Introduction

The way to prove a physical theory is to compare its predictions with the observations. This has been the case with the cosmological models where effects such as the red shift or the homogeneous background radiation constitute observations in

J. Phys. B: At. Mol. Opt. Phys. **42** (2009) 154009

Review

accordance with a description of an expanding universe and the particle creation. But to perform a truly cosmological experiment is out of the reach of our current technology, in particular one that reproduces the early stages of the universe characterized with an extremely high energy density and a rapid expansion.

In other cases like with relativistic particles, it is possible to make experiments where electrons for example are driven to almost the speed of light. But some interesting effects are still out of reach of our measurement capabilities, for example the *Zitterbewegung*, predicted from the Dirac equation. It states that a freely moving spin-1/2 particle, in absence of external potentials, is subject to a helicoidal motion around the main direction of propagation. Another counterintuitive effect, the Klein paradox (Klein 1929), states that an electron could transmit unimpeded through a potential barrier. But this effect has not yet been observed with elementary particles.

6.2. Simulating the Unruh effect

6.2.1. Methods. Following the work of Unruh (1976), it was shown that in the vacuum of a Minkowski (flat) universe an accelerated observer would measure a thermal spectrum of particles whose temperature is proportional to his acceleration. Later, this effect was generalized by Gibbons and Hawking (1977) for a curved de Sitter space. The de Sitter space is a massless curved spacetime that is isotropic and homogeneous in space and that looks like the Minkowski space locally (Bergström and Goobar 2004). The de Sitter space is also a cosmological model that describes an exponential expansion of the universe due to a non-vanishing and positive cosmological constant Λ.

The scalar field describing a massless inflating universe with a single global mode can be imitated by the quantized motion of a single ion around its equilibrium position. The phonon excitations of the ion would simulate the field quanta of the universe. The ion itself can be used as a detector by coupling its vibrational state to an easily readable internal state.

In the case of an expanding de Sitter universe, a comoving quanta field detector would experience a Doppler frequency shift of the form $\nu(t)^{\Lambda} = \nu_0^{\Lambda} \exp\left(-\sqrt{3\Lambda}t\right)$ (Birrell and Davies 1984). The spectrum measured with this detector is equivalent to that measured by a thermally excited inertial detector with a temperature $T = \hbar\sqrt{3\Lambda}/k_{\mathrm{B}}$ (Gibbons and Hawking 1977).

In the case of a single ion trapped in a time-dependent potential that varies in the trap frequency $\nu(t) = \nu_0 \exp\left(-\kappa t\right)$, a similar effect can be measured. A pseudo-temperature of $k_{\mathrm{B}}T = \hbar\kappa/2\pi$ is associated with the average occupation number of the vibrational energy levels.

The coupling between internal and vibrational states of the ion can be created by a laser field described in the dipole and rotating wave approximation by the interaction-picture Hamiltonian (Alsing *et al* 2005, James 1998):

$$H_{\mathrm{I}} = \hbar\Omega k z(t)[\sigma^- \mathrm{e}^{-\mathrm{i}\Delta t} - \sigma^+ \mathrm{e}^{\mathrm{i}\Delta t}]. \tag{58}$$

Here, σ^+ and σ^- are the raising and lowering spin-1/2 operators, respectively, Δ is the detuning of the laser relative to the atomic transition and Ω is the Rabi frequency. The laser

wave vector $\vec{k}$ points along the direction in which the ion's vibrational motion is excited (here the z-direction). We assume an anisotropic trap (e.g. a linear trap) where, by choosing the detuning Δ and the wave vector $\vec{k}$, the experimenter can control which vibrational motion to excite.

The evolution of the position operator $z(t)$ is deduced by solving the equations of motion of the ion in its harmonic trap neglecting its coupling with the light field. In the Heisenberg representation and with

$$H = \frac{p^2}{2m} + \frac{m}{2}\nu(t)^2 z^2, \tag{59}$$

we have (Menicucci and Milburn 2007)

$$\dot{z} = -\frac{\mathrm{i}}{\hbar}[H, z] = \frac{p_z}{m}$$
$$\dot{p}_z = -\frac{\mathrm{i}}{\hbar}[H, p_z] = m\nu(t)^2 z. \tag{60}$$

After the opening of the harmonic potential $\nu(t)$ during a time T in which the interaction is on, a vibrational phonon can be mapped into the excited $|1\rangle$ internal state. The probability of exciting the internal state of the ion calculated with first order perturbation theory and in the slow- $\kappa \ll \nu_0$ and long-time $\nu_0 \mathrm{e}^{-\kappa T} \ll \kappa$ frequency variations for the trap potential is (Menicucci and Milburn 2007),

$$P^{(1)}(\Delta) = \frac{1}{\hbar^2} \int_0^T \mathrm{d}t_1 \int_0^T \mathrm{d}t_2 \langle 0| H_{\mathrm{I}}(t_1) |1\rangle \langle 1| H_{\mathrm{I}}(t_2) |0\rangle$$
$$= (\Omega\eta_0)^2 \frac{2\pi\nu_0}{\kappa\Delta^2} \frac{1}{\left(\mathrm{e}^{2\pi\Delta/\kappa} - 1\right)^2}. \tag{61}$$

When the trap is opened to simulate the expansion of the universe, the ion is used as a detector to measure the thermal spectrum from the phonon distribution. A particular case is when the laser is in resonance with the red sideband ($\Delta \approx \nu$). The ion acts like a phonon detector that absorbs the measured particle (together with a photon) in order to produce an internal excitation of the ion. When the laser is in resonance with a blue sideband ($\Delta \approx -\nu$), the ion acts like an unconventional detector that emits a phonon to get excited. The ratio of the excitation probabilities gives the experimental signature of the ion thermal distribution (Wineland and Itano 1979, Monroe *et al* 1995b),

$$\frac{P_{\mathrm{red}}}{P_{\mathrm{blue}}} = \frac{\bar{n}}{\bar{n}+1} = \mathrm{e}^{-\hbar\nu_0/k_{\mathrm{B}}T}, \tag{62}$$

where $\bar{n}$ is the average phonon occupation value. From the excitation probabilities of equation (61), the ratio of the red to the blue sidebands is given by Menicucci and Milburn (2007):

$$\frac{P^{(1)}(\Delta)}{P^{(1)}(-\Delta)} = \mathrm{e}^{-2\pi\Delta/\kappa}. \tag{63}$$

Therefore, the temperature associated with the exponential opening of the trap potential is given by $T = \hbar\kappa/2\pi k_{\mathrm{B}}$. This temperature is equivalent to the Gibbons–Hawking temperature $T = \hbar\sqrt{3\Lambda}/k_{\mathrm{B}}$ (Gibbons and Hawking 1977).

The increase of the temperature of the trapped ion is due to the trap opening. At the beginning of the trap opening, the evolution is adiabatic since the trap frequency obeys the condition $|\dot{\nu}|/\nu \ll \nu$. Indeed, the expansion constant was

selected small compared to the initial trap frequency $\kappa \ll \nu_0$. At a later time T chosen following the condition $\nu_0 e^{-\kappa T} \ll \kappa$, the evolution turns to be non adiabatic. Indeed, the trap frequency is going to be so weak that even a small rate of change would be non-adiabatic. The ion that was initially in the ground state is excited to higher vibrational levels because of the non-adiabatic reduction of the confining potential.

6.2.2. Experiment. In this case, we measure the temperature associated with the ion phonon distribution. This temperature is related to the Gibbons–Hawking temperature.

To perform this experiment, a single trapped ion is cooled to the vibrational ground state level. Next, the ion is pumped into its electronic ground level that is related to the vacuum state of the universe. Then, the trap potential, initially at the frequency ν_0, is exponentially reduced $\nu(t) = \nu_0 \exp(-\kappa t)$. During the opening of the trap, Raman laser beams between hyperfine levels or a narrow frequency laser tuned to a quadrupole transition are set in resonance with the red or the blue sideband. It should be noted that the coupling field must be in resonance with the sideband during the trap opening. After some time, the ion internal state is measured by fluorescence using the shelving technique with the help of an additional laser beam in resonance with the excited internal state.

The trap potential is then raised and the sequence can be repeated for the opposite sideband. The height of the red and blue sidebands is compared and the temperature dependence on the trap expansion coefficient κ is measured.

A typical value of the initial trap frequency $\nu_0 \simeq 1$ MHz can be used to perform this experiment. Therefore, the expansion coefficient can be selected like $\kappa \simeq 1$ kHz and the expansion time T of several ms. These are typical parameters in current ion-trap experiments.

Difficulties that may arise when performing such an experiment are associated with unwanted heating of the ion caused, first, by a possible unintentional displacement of the trap minimum and by anharmonic terms in the trap potential and, second, by fluctuating patch potentials. The former could be solved by compensating for the anharmonicities and the displacement of the trap potential by tuning appropriate compensating fields for every value of the time-varying trap frequency. The latter could be overcome by performing the experiment during a short enough time so that the heating can be neglected.

6.3. Simulating the cosmological particle creation

6.3.1. Methods. The standard model describes the particle creation from the vacuum fluctuations during the early stages of the universe. Since the expansion of the universe is non-adiabatic, an initial ground state will be excited evolving into a squeezed state of entangled pairs of particles. The created particle pairs are simulated by entangled phonon pairs created by the excitation of the ground ionic motional level as the trap potential is non-adiabatically varied.

One can use a real massless scalar field ϕ as an approximation to describe an expanding or contracting universe. Using the Friedman–Lemaître–Robertson–Walker metric (Birrell and Davies 1984), $ds^2 = a^6(t) dt^2 - a^2(t) dr^2$,

one finds that the wave equation describing the universe reads as (Schützhold *et al* 2007)

$$\left(\frac{\partial^2}{\partial t^2} + [a^4(t)\mathbf{k}^2 + \zeta a^6(t)\Re(t)] \right) \phi_{\mathbf{k}} = 0, \tag{64}$$

where the Ricci (curvature) scalar $\Re$ is coupled to the field via the dimensionless parameter ζ. Each mode $\mathbf{k}$ represents a harmonic oscillator with a time-dependent potential $a^4(t)\mathbf{k}^2 + \zeta a^6(t)\Re(t)$.

In the case of a chain of ions trapped in a transversally strongly confining linear trap with a time-dependent axial trap frequency $\nu_z(t)$, the position z_i of the ith ion follows the equation of motion

$$\ddot{z}_i + \nu_z^2(t)z_i = \gamma \sum_{j \neq i} \frac{\text{sign}(i-j)}{(z_i - z_j)^2}. \tag{65}$$

This equation can be solved classically by the use of the scaling ansatz

$$z_i(t) = b(t)z_i^0, \tag{66}$$

where z_i^0 are the initial equilibrium positions. The scaling factor $b(t)$ evolves following

$$\left(\frac{\partial^2}{\partial t^2} + \nu_z^2(t) \right) b(t) = \frac{\nu_z^2(t=0)}{b^2(t)}. \tag{67}$$

The quantum fluctuations are introduced by splitting the position operator $\hat{z}_i$ into its classical evolution $b(t)z_i^0$ and a quantum fluctuation term $\delta\hat{z}_i(t)$:

$$\hat{z}_i(t) = b(t)z_i^0 + \delta\hat{z}_i(t). \tag{68}$$

Replacing equation (68) in equation (65) and later linearizing over $\delta\hat{z}_i(t)$ (since the displacement of the ions can be assumed small), one obtains after normal mode expansion (Schützhold *et al* 2007)

$$\left(\frac{\partial^2}{\partial t^2} + \left[\nu_z^2(t) + \frac{\nu_\kappa^2}{b^3(t)} \right] \right) \delta\hat{z}_\kappa = 0 \tag{69}$$

for the phonon modes κ. One can recognize the similarities between equations (64) and (69). The scalar field $\phi_{\mathbf{k}}$ behaves in the same way as the quantum fluctuation of the ions (phonon) $\delta\hat{z}_\kappa$, and each mode $\mathbf{k}$ of the field has a direct analogy with the phonon frequency of the ions ν_κ.

It has been shown that a non-adiabatic change in the trap potential can create squeezed states (Heinzen and Wineland 1990).

6.3.2. Experiment. The simulation can be performed in a system composed of, for example, two hyperfine states $|0\rangle$ and $|1\rangle$ of an ion. The states should be coupled by a two-photon Raman transition or by an rf field in the presence of a magnetic gradient. Note that the pairs of Raman beams or the rf field couple not only the two hyperfine states $|0\rangle$ and $|1\rangle$, but also the vibrational levels of the ion $|n\rangle = (|n=1\rangle, |n=2\rangle, \ldots)$. For this simulation, one uses three different coupling fields: one coupled to the second red sideband $|0, n+2\rangle \rightarrow |1, n\rangle$ (*a*), another to the first red sideband $|0, n+1\rangle \rightarrow |1, n\rangle$ (*b*), and the last one to the carrier transition $|0, n\rangle \leftrightarrow |1, n\rangle$ (*c*). An additional level $|e\rangle$ is used for fluorescence detection of the population in level $|0\rangle$. The laser pulse (*d*) $|0\rangle \rightarrow |e\rangle$ drives a
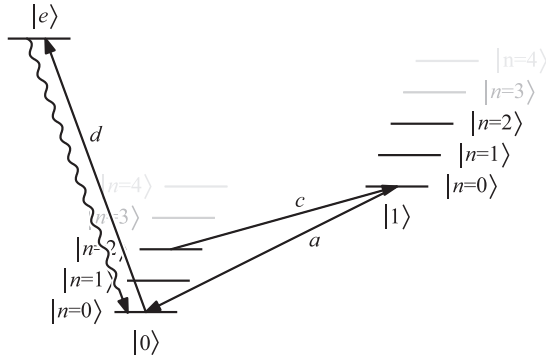
Figure 13. A possible energy level diagram and the transitions used to measure the population in the $n = 2$ level. If the ion is found in level $|0, n = 2\rangle$ after the trap contraction, then applying a π second red sideband pulse (c) followed by a π carrier pulse (a) brings the ion to the state $|0, n = 2\rangle$. When the ion is in this latter level, fluorescence can be seen by using the detection laser (d). In contrast if the ion is initially in $|0, n = 0\rangle$ or $|0, n = 1\rangle$, the first pulse (c) would not change the state of the ion since it does not have enough energy to be in resonance with the $|1\rangle$ energy level but the subsequent carrier pulse (c) transfers the population to the corresponding vibrational levels of $|1\rangle$. Then no fluorescence can be seen when the detection laser (d) is applied. Note that the transitions (a) and (c) should be narrow enough not to couple the adjacent vibrational levels and that the detection laser drives a dipole transition that couples many of the vibrational levels.

dipole transition that does not resolve the vibrational levels as the Raman beams or rf field do.

A non-adiabatic increase of the strength of trap potential confining the ion will simulate the universe expansion. After non-adiabatically changing the trap potential, the ions motional state will be a squeezed state where only even (i.e. symmetric with respect to the trap minimum) vibrational levels contribute. Thus, the signature of the squeezed state is the population of even vibrational levels. Measuring the population of the $|n = 2\rangle$ vibrational level should be sufficient, since the population in higher vibrational levels is expected to be negligible. In order to measure the population of the $n = 2$ state, one performs a series of pulses described in figure 13 that couple the motional state to the easily readable internal state of the ion.

Since cooling is more efficient for strong confinement, it is advantageous to begin with a strongly confining potential and cool to the ground state of motion. Then, after an adiabatic lowering of the trap potential it is ramped back up non-adiabatically to its initial strength.

To discriminate against any classical heating, i.e. parametric or other classical perturbations, the probability of populating the $n = 1$ level can be measured in a similar way as shown in figure 13. The comparison between both probabilities gives the proof that a squeezed state is generated, if a higher probability for populating the $n = 2$ level than $n = 1$ is obtained.

6.4. Simulating the Dirac equation

6.4.1. Methods. Relativistic effects related to the solution of the Dirac equation can be simulated in trapped ion systems as

proposed in Bermudez *et al* (2007) and Lamata *et al* (2007), in particular phenomena such as the *Zitterbewegung* (helicoidal motion of the free Dirac particle as a consequence of the non-commutativity of its velocity operator components) or the Klein paradox (transmission of a relativistic particle of mass m through a potential edge of height $V > 2mc^2$ with nearly no reflection).

In order to simulate the Dirac equation in (3+1) dimensions for a spin-1/2 particle in a single trapped ion, Lamata *et al* (2007) proposed to design a Hamiltonian that reproduces the same dynamics. For a free electron in three dimensions, the Dirac formalism uses a bispinor that is a vector-valued wavefunction of four components. In order to represent all the components, one can use a four-level system with states $|a\rangle, |b\rangle, |c\rangle, |d\rangle$ that correspond to four internal levels of the ion respectively. The bispinor is defined as (Lamata *et al* 2007)

$$|\Psi\rangle := \Psi_a |a\rangle + \Psi_b |b\rangle + \Psi_c |c\rangle + \Psi_d |d\rangle = \begin{pmatrix} \Psi_a \\ \Psi_b \\ \Psi_c \\ \Psi_d \end{pmatrix}. \quad (70)$$

The dynamic of the system is generated by the pairwise coupling of the internal levels with the centre-of-mass vibrational levels whose energies are determined by the trap frequencies ν_x, ν_y, ν_z. Again, three common types of interaction are used. A carrier interaction coherently couples two ionic internal levels without changing the external motion of the ion, for example $|a, n\rangle \leftrightarrow |c, n\rangle$. Jaynes–Cummings (JC) and anti-Jaynes–Cummings (AJC) interactions resonantly couple the ionic internal with the vibrational levels. The former induce the red sideband transition and the latter the blue one, for example $|a, n + 1\rangle \leftrightarrow |c, n\rangle$ and $|a, n\rangle \leftrightarrow |c, n + 1\rangle$ respectively. The corresponding interaction Hamiltonians under the rotating wave and Lamb–Dicke approximations are

$$\begin{aligned} H_\sigma &= \hbar\Omega(\sigma^+ e^{i\phi} + \sigma^- e^{-i\phi}) \\ H_r &= \hbar\eta\tilde{\Omega}(\sigma^+ a\, e^{i\phi_r} + \sigma^- a^\dagger e^{-i\phi_r}) \\ H_b &= \hbar\eta\tilde{\Omega}(\sigma^+ a^\dagger e^{i\phi_b} + \sigma^- a\, e^{-i\phi_b}) \end{aligned} \quad (71)$$

Here again σ^+ and σ^- are the raising and lowering ionic spin-1/2 operators, $a^\dagger$ and a are the creation and annihilation operators associated with the motional state of the ion and $\eta = \sqrt{\hbar k^2/2M\nu}$ is the Lamb–Dicke parameter. The Rabi oscillation frequencies for the blue and red sideband transitions were set to the same value $\tilde{\Omega}$ and to Ω for the carrier transition.

When only the carrier coupling is applied, with the appropriate choice of the phase ϕ, one obtains

$$H_{\sigma_j} = \hbar\Omega_j\sigma_j \quad (72)$$

with $j = \{x, y\}$ and σ_j being the Pauli matrices.

When the blue and red sideband couplings are used simultaneously, the resulting Hamiltonian is the sum of H_r and H_b from equation (71). By choosing the phases of the sideband fields such as $\phi_b - \phi_r = \pi$, one obtains

$$H_{\sigma_j}^p = \pm i\hbar\eta\Delta\tilde{\Omega}\sigma_j(a - a^\dagger). \quad (73)$$

Here, $\Delta = \sqrt{\hbar/2M\nu}$ is the spread in the position of the ground wavefunction. The operator σ_j is the Pauli matrix
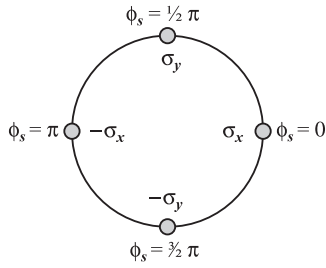
Figure 14. The selection of the phases of the red and blue sideband ϕ_r and ϕ_b fields are important since they shape the form of the Hamiltonian. In particular, the sum of the phases $\phi_s = (\phi_r + \phi_b)/2$ defines the direction of the spin operator and also the global sign of the Hamiltonian (73).

along the $j = \{x, y\}$ component of the spin. It is not related to the vibrational directions of motion but to the ionic internal transitions.

The selection of the Pauli matrix $\sigma_x = \sigma^+ + \sigma^-$ or $\sigma_y = i(\sigma^- - \sigma^+)$ as well as the sign of the Hamiltonian is performed by an additional condition of the applied red and blue sideband phases. Even if a condition on their difference was already used, one needs a supplementary condition to completely define the phases. The sum of the phases of the applied fields $\phi_s = (\phi_b + \phi_r)/2$ determines the sign of the Hamiltonian, negative for $\phi_s = \{\pi, 3/2\pi\}$ and positive for $\phi_s = \{0, 1/2\pi\}$, whereas the Pauli matrix σ_j is selected along $j = x$ for $\phi_s = \{0, \pi\}$ and along $j = y$ for $\phi_s = \{\pi/2, 3/2\pi\}$ (see figure 14). The phase ϕ_s itself does not modify the dynamics of the system when the previous Hamiltonian is considered alone, but it is essential to build the Dirac-like Hamiltonian composed of many element couplings as in equation (73). The dynamics of equation (73) are based on a spin-dependent coupling between the internal and vibrational states that can also be used for the creation of entangled states of spin and motion. This coupling has already been applied in previous experiments (Haljan *et al* 2005, Sackett *et al* 2000).

The Hamiltonian of equation (73) constitutes the basic block to construct the Dirac Hamiltonian in (3+1) dimensions. Since the spin-1/2 particle to simulate has a momentum with components in all three spatial directions, one needs to consider Hamiltonian terms along all of these directions. The operators $a^\dagger$ and a can be associated with the three normal trap frequencies and therefore with the motion along the three trap axes. One needs to distinguish $a^\dagger_\ell$ and a_ℓ for every axis $\ell = x, y, z$. The same consideration should be made for the Lamb–Dicke parameter η_ℓ, the spread in the position of the ground-state wavefunction Δ_ℓ and the Rabi frequency Ω_ℓ that also needs to be defined along the direction of the applied interaction. The difference between the creation and annihilation operators can be written in terms of the momentum operator $p_\ell = i\hbar(a^\dagger_\ell - a_\ell)/\Delta_\ell$. Following previous considerations, the Hamiltonian of equation (73) can be rewritten as

$$H^{p_\ell}_{\sigma_j} = 2\eta_\ell \Delta_\ell \tilde{\Omega}_\ell \sigma_j p_\ell. \tag{74}$$

In order to simulate the Dirac dynamics employing four internal states of an ion, the transitions $|a\rangle \leftrightarrow |c\rangle$, $|a\rangle \leftrightarrow |d\rangle$, $|b\rangle \leftrightarrow |c\rangle$ and $|b\rangle \leftrightarrow |d\rangle$ are employed. The

corresponding spin-1/2 operators of equation (74) need to be defined for the specific transition $\sigma^{ac}_j, \sigma^{ad}_j, \sigma^{bc}_j$ and σ^{bd}_j, and therefore the corresponding Hamiltonians from equation (74) can be written as $H^{p_\ell}_{\sigma_j(ac)}, H^{p_\ell}_{\sigma_j(ad)}, H^{p_\ell}_{\sigma_j(bc)}$ and $H^{p_\ell}_{\sigma_j(bd)}$. In the case of the carrier interaction of equation (72) two internal transitions are used, giving the following Hamiltonians $H_{\sigma_\ell(ac)}$ and $H_{\sigma_\ell(bd)}$.

With the correct selection of the direction and phase for the different fields, one can tailor the desired Hamiltonian as a linear combination of H_{σ_ℓ} and $H^{p_\ell}_{\sigma_j}$ yielding, for instance (Lamata *et al* 2007),

$$H_D = H^{p_x}_{\sigma_x(ad)} + H^{p_x}_{\sigma_x(bc)} + H^{p_y}_{\sigma_y(ad)} - H^{p_y}_{\sigma_y(bc)}$$
$$+ H^{p_z}_{\sigma_x(ac)} - H^{p_z}_{\sigma_x(bd)} + H_{\sigma_y(ac)} + H_{\sigma_y(bd)}. \tag{75}$$

It should be noted that all the Rabi oscillation frequencies for the sideband and carrier transitions $\tilde{\Omega}$ and Ω, the spread in position Δ and the Lamb–Dicke parameter η are selected equal in all the components of the previous Hamiltonian for reasons that will be explained later. This means that the fields employed to drive the various couplings should have the same relative strength for all the directions of space, and the ion trap should be spherical. Therefore, one may obtain a Hamiltonian H_D that is symmetric with respect to all directions of space. The Hamiltonian H_D can be written in a 4×4 matrix representation in a base defined by the four internal states of the ion (see equation (70)):

$$H_D = \begin{pmatrix} 0 & 2\eta\Delta\tilde{\Omega}(\vec{\sigma} \cdot \vec{p}) - i\hbar\Omega \\ 2\eta\Delta\tilde{\Omega}(\vec{\sigma} \cdot \vec{p}) + i\hbar\Omega & 0 \end{pmatrix}, \tag{76}$$

where each element represents a 2×2 matrix. This Hamiltonian can be compared with the 'supersymmetric' representation of the Dirac Hamiltonian (Thaller 1992),

$$H_D = \begin{pmatrix} 0 & c(\vec{\sigma} \cdot \vec{p}) - imc^2 \\ c(\vec{\sigma} \cdot \vec{p}) + imc^2 & 0 \end{pmatrix}. \tag{77}$$

The speed of light c and the electron rest energy mc^2 are related to the coupling strengths Ω and $\tilde{\Omega}$ following

$$c = 2\eta\Delta\tilde{\Omega} \qquad \text{and} \qquad mc^2 = \hbar\Omega. \tag{78}$$

The previous selection of symmetric couplings applied along all the directions of space represents in a simulation the isotropy of the velocity of light.

One can recognize the similarities between these two Hamiltonians, making possible the simulation of a quantum relativistic evolution of a spin-1/2 particle with an ion-trap experiment.

If the dynamics created by the Hamiltonian of equation (76) were reproduced in an experiment with a four-level system using Raman beams, it would require 14 pairs of Raman lasers, two for each element of the form $H^{p_\ell}_{\sigma_j}$ (see equation (74)) and one for each carrier element H_{σ_ℓ} (see equation (72)). Of course, some simplifications can be applied, such as modulating the frequency of the beams to generate the blue and the red sideband transitions with a single pair of beams. But the need of controlling their phases independently and the minimal requirement of having at least two pairs of beams (modulated in frequency) with a resulting
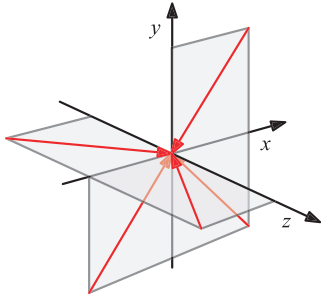
Figure 15. Possible laser configuration to build the Dirac Hamiltonian with Raman transitions. In order to build a symmetric Hamiltonian such as that of equation (76), the wave vectors must be the same along the three trap axes. For simplification of the lasers requirements, only one wavelength can be used. Then the four levels to perform the simulation need to be close enough in energy, i.e. two Zeeman split hyperfine levels as proposed in Lamata *et al* (2007). Therefore, the angles subtended by every pair of Raman beams must be the same. Additionally, the beams need to be modulated with the correct frequency to drive the desired transitions.

k-vector along each one of the trap axes should be stressed (see figure 15).

In order to render the simulation achievable with current experiments, one can simplify the (3+1)-dimensional Hamiltonian of equation (77) and work with (2+1) dimensions (Bermudez *et al* 2007) or simplify even more to (1+1) dimensions that still reproduce the most important effects of the Dirac equation. The resulting (1+1)-dimensional Hamiltonian becomes, after a $\pi/2$ rotation around the x-axis that changes σ_y into σ_z (Lamata *et al* 2007),

$$H_{\mathrm{D}}^{(1)} = 2\eta\Delta\tilde{\Omega}\sigma_x p_x + \hbar\Omega\sigma_z. \tag{79}$$

This Hamiltonian operates on the Dirac 'spinor' $|\Psi^{(1)}\rangle = \Psi_a^{(1)}|a\rangle + \Psi_b^{(1)}|b\rangle$ built with a positive $\left(\Psi_a^{(1)}\right)$ and a negative $\left(\Psi_b^{(1)}\right)$ kinetic energy component (Thaller 1992). The term $2\eta\Delta\tilde{\Omega}\sigma_x p_x$ results from the application of blue and red sideband fields. It is just the sum of H_{b} and H_{r} with phases $\phi_{\mathrm{b}} = -\pi/2$ and $\phi_{\mathrm{r}} = \pi/2$. The last term $\hbar\Omega\sigma_z$ can be obtained, for instance, by applying an off-resonant laser pulse that induces an ac-Stark shift. Because of the reduction to one spatial dimension, the trapping potential should also be one dimensional, that is, a linear trap with strong radial confinement compared to the axial one would be well suited.

The experimental requirements for simulating the (1 + 1) Dirac Hamiltonian are substantially reduced and achievable in current experiments.

6.4.2. Experiment for the simulation of the Zitterbewegung. By numerically solving the Dirac equation, it is possible to visualize the peculiar behaviour of the probability density function. One of these peculiarities is the Zitterbewegung where the position of a particle oscillates even in the absence of external potentials. Usually, this relativistic effect is not seen in experiments since the frequency is on the order 10^{21} Hz and the amplitude on order 10^{-3} Å for a real particle such as an electron.

When simulating the Zitterbewegung with trapped ions, the frequency and amplitude of the oscillatory motion for an ion with average momentum p_0 are given by Lamata *et al* (2007):

$$\omega_{\mathrm{ZB}} \approx \sqrt{2\eta^2\tilde{\Omega}^2 p_0^2/\hbar^2 + \Omega^2}, \tag{80}$$

$$R_{\mathrm{ZB}} = \frac{\eta\hbar^2\tilde{\Omega}\Omega\Delta}{4\eta^2\tilde{\Omega}^2\Delta^2 p_0^2 + \hbar^2\Omega^2}. \tag{81}$$

From equation (80), one can obtain a measurable output with frequencies ranging from zero to some megahertz and amplitudes that can go to a thousand Angstroms varying the typical parameters of Rabi frequencies and trap depths. It can be noted that the amplitude of the Zitterbewegung can be made independent of the Rabi frequencies if $\eta\tilde{\Omega} \approx \Omega$ indicating that this effect could even be seen with small laser fields.

In order to observe the Zitterbewegung, one needs to determine the momentum and the position of the ion for different times. In previous experiments (Meekhof *et al* 1996a, 1996b), the state of motion of the ion was determined by measuring the population distribution of the Fock states. From the red sideband excitation probability as a function of time, one can fit the different frequency components associated with the contribution of every vibrational level. Therefore, the determination of the distribution over Fock vibrational states requires many data points. Another possibility could be to measure the Wigner function by instantaneous measurements, even in the presence of a thermal bath, based on the proposal in Santos *et al* (2007).

To reduce the number of data points to acquire, one can just measure the expected value of the generalized quadrature $Y_\phi = (a\mathrm{e}^{-\mathrm{i}\phi} - a^\dagger\mathrm{e}^{\mathrm{i}\phi})/2$ as proposed by Lougovski *et al* (2006). Indeed one does not need to measure the whole wavefunction to know the position or momentum of the ion; it is enough to measure the expected value. The angle ϕ is related to the internal spin state $|+_\phi\rangle = (|a\rangle + \mathrm{e}^{\mathrm{i}\phi}|b\rangle)$ where the ion is initialized. Additionally, a JC interaction needs to be applied (see H_{r} in equation (71)) which couples the vibrational state to the internal state where the measurement is performed.

The probability P_b of finding the ion in the state $|b\rangle$ is given by (see Bastin *et al* 2006)

$$\frac{\mathrm{d}}{\mathrm{d}t}P_b = \frac{1}{\mathrm{i}\hbar}\langle[|b\rangle\langle b|, H_0 + H_{\mathrm{r}}]\rangle + \left\langle\frac{\partial}{\partial t}|b\rangle\langle b|\right\rangle$$

$$= \frac{1}{\mathrm{i}\hbar}\langle[|b\rangle, H_{\mathrm{r}}]\rangle. \tag{82}$$

The state of the ion at time $t = t_0$ is given by $\rho_{\mathrm{m}}(t_0)\otimes|+_\phi\rangle\langle+_\phi|$, where ρ_m is the density matrix for the vibrational levels. Then the probability of finding the ion in state $|b\rangle$ at time $t = t_0$ is given by

$$\frac{\mathrm{d}}{\mathrm{d}t}P_b\bigg|_{t=t_0} = \frac{1}{\mathrm{i}\hbar}\langle[|b\rangle\langle b|, H_{\mathrm{r}}]\rangle|_{t=t_0}$$

$$= \mathrm{Tr}\left[\rho_{\mathrm{m}}(t_0)\otimes|+_\phi\rangle\langle+_\phi||b\rangle\langle b|, H_{\mathrm{r}}]\right]$$

$$= \eta\tilde{\Omega}\langle Y_\phi\rangle. \tag{83}$$

Therefore, the generalized quadrature can be written in dimensionless time $\tau = \eta\tilde{\Omega}t$ as

$$\langle Y_\phi\rangle = \frac{\mathrm{d}}{\mathrm{d}\tau}P_b^{+_\phi}\bigg|_{\tau=0}. \tag{84}$$

When choosing $\phi = -\pi/2$ and $\phi = 0$ the position and momentum operators are measured, respectively. Note that only two measurements of the probability of finding the ion in state $|b\rangle$ are needed to be taken to determine the position or momentum of the ion.

In order to perform the simulation of the Zitterbewegung the ion can be cooled to the vibrational ground level, although it is not required, since it is also possible to measure the Zitterbewegung of a Doppler-cooled ion. Then the internal state of the ion is set to $|a\rangle$. The next step is to excite the ion to a given motional state, i.e. a Fock state (Meekhof *et al* 1996a, 1996b), a coherent state (Carruthers and Nieto 1965), a thermal state (Stenholm 1986), a squeezed state (Heinzen and Wineland 1990, Cirac *et al* 1993) or an arbitrary state. The relativistic-like dynamic ruled by the interaction H_D (see equation (79)) is generated by turning on the fields resonant with the blue and red sidebands at time $t = 0$. The time evolution of the ion ends at $t = t_0$ when the interaction generated by the Hamiltonian H_D is turned off. Simultaneously, the internal state of the ion is driven to $|+_\phi\rangle$ by the application of an external field; then a JC coupling (see H_r in equation (71)) is applied to map the ion motional state into its internal state. At time $t = t_0 + \tau$ with $\tau \ll 2\pi/\omega_{ZB}$, the population in the level $|b\rangle$ is measured by detecting resonance fluorescence. The previous sequence is repeated with the same parameters for a given number of repetitions to find the probability $P_b^{+_\phi}(t_0 + \tau)$. Then, the probability $P_b^{+_\phi}$ at $t = t_0$ is also measured (without the need of applying the JC coupling). From the two last probabilities, the expectation of the generalized quadrature can be deduced. The whole sequence is then repeated for different t to extract the trajectory of the ion.

6.4.3. Experiment of the simulation of the Klein paradox. The Klein paradox (Klein 1929) is a relativistic effect described by the Dirac equation. It states that an electron can be transmitted with almost no reflection through a potential step with a height V bigger than twice the electron rest energy mc^2.

In the Dirac formalism, the particle kinetic energy E takes into account the rest mass and therefore the electron momentum is given by

$$p = \frac{1}{c}\sqrt{(E-V)^2 - m^2 c^4}. \tag{85}$$

When $|E - V| < mc^2$, the momentum is imaginary and the wavefunction exponentially decays. However, when $V \geqslant E + mc^2$, the momentum is real and one obtains a transmitted wave. This solution lies in the negative kinetic energy range $E < -mc^2 + V$ and is therefore associated with electron–positron pair production. The positron sees an inverted potential step and therefore its motion is not impeded (see figure 16).

The transmission through a potential step can be reproduced by the Hamiltonian,

$$H_V^{(1)} = H_D^{(1)} + V(|a\rangle\langle a| + |b\rangle\langle b|). \tag{86}$$

The last term is the potential step $V(|a\rangle\langle a| + |b\rangle\langle b|)$ that is set at time $t = t_0$. It can be implemented for example by the use
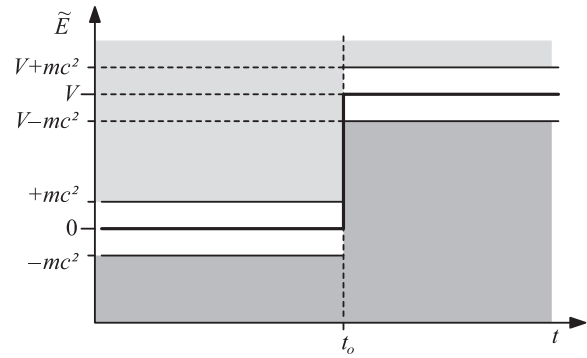
Figure 16. Potential step (thick line). The white areas represent the forbidden regions where the solutions of the Dirac equation are exponentially decaying. The light and dark gray areas correspond to the positive and negative energy regions respectively. An electron with energy $mc^2 < E < V - mc^2$ is found initially in the positive energy region. For $t > t_0$, after the potential step, the energy lies in the negative energy region allowing the creation of a hole in the Dirac sea. Picture adapted from Schwabl (1997).

of a detuned laser that produces the same Stark shift in both levels.

The experimental protocol is summarized in the following steps. First, the ions are cooled to the ground state $|a\rangle$. Then the JC and AJC couplings, described in equation (79), are applied at $t = 0$ by turning on the red and blue sideband excitation fields. Next, the potential step is turned rapidly on at time $t = t_0$. Last, the population in the state $|b\rangle$ is measured by fluorescence. The probability of finding the ion in the state $|b\rangle$ is obtained after several repetitions and is equivalent to the transmission probability through the step potential.

Acknowledgments

References

Alsing P M, Dowling J P and Milburn G J 2005 *Phys. Rev. Lett.* **94** 220401–4
Amico L, Fazio R, Osterloh A and Vedral V 2008 *Rev. Mod. Phys.* **80** 517–60
Anderson M H, Ensher J R, Matthews M R, Wieman C E and Cornell E A 1995 *Science* **269** 198–201
Aubry S and Le Daeron P Y 1983 *Physica* D **8** 381–422
Bardeen J, Cooper L N and Schrieffer J R 1957 *Phys. Rev.* **108** 1175
Barjaktarevic J P, Milburn G J and McKenzie R H 2005 *Phys. Rev.* A **71** 012335
Barrett M D *et al* 2004 *Nature* **429** 737–9
Bastin T, von Zanthier J and Solano E 2006 *J. Phys. B: At. Mol. Opt. Phys.* **39** 685–93
Bergström L and Goobar A 2004 *Cosmology and Particle Astrophysics* 2nd edn (Chichester: Praxis Publishing)
Bermudez A, Martin-Delgado M A and Solano E 2007 *Phys. Rev. A* **76** 041801–4
Birkl G, Kassner S and Walther H 1992 *Nature* **357** 310–3

Birrell N D and Davies P C W 1984 *Quantum Fields in Curved Space (Cambridge Monographs on Mathematical Physics)* (Cambridge: Cambridge University Press)

Blatt R and Wineland D 2008 *Nature* **453** 1008–15

Borgonovi F, Guarneri I and Shepelyansky D L 1989 *Phys. Rev. Lett.* **63** 2010

Braun O M and Kivshar Y S 1998 *Phys. Rep.* **306** 1–108

Braun O M and Kivshar Y S 2004 *The Frenkel–Kontorova Model: Concepts, Methods, and Applications* (Berlin: Springer)

Braungardt S, Sen A, Sen U and Lewenstein M 2007 *Phys. Rev. A* **76** 042307–9

Brüser D submitted

Brush S G 1967 *Rev. Mod. Phys.* **39** 883

Cai J, Popescu S and Briegel H J 2008 arXiv:0809.4906

Carruthers P and Nieto M M 1965 *Am. J. Phys.* **33** 537

Chiaverini J and Lybarger W E 2008 *Phys. Rev. A* **77** 11

Ciaramicoli G, Galve F, Marzoli I and Tombesi P 2005 *Phys. Rev. A* **72** 042323

Ciaramicoli G, Marzoli I and Tombesi P 2007 *Phys. Rev. A* **75** 032348

Ciaramicoli G, Marzoli I and Tombesi P 2008 *Phys. Rev. A* **78** 012338

Cirac J I, Parkins A S, Blatt R and Zoller P 1993 *Phys. Rev. Lett.* **70** 556

Cirac J I and Zoller P 1995 *Phys. Rev. Lett.* **74** 4091

Cirac J L and Zoller P 2000 *Nature* **404** 579–81

Clark R J, Lin T, Brown K R and Chuang I L 2008 arXiv: 0809.2824v1 [quant-ph]

Das A and Chakrabarti B K 2005 *Quantum Annealing and Related Optimization Methods (Lecture Notes in Physics)* (Berlin: Springer)

Davis K B, Mewes M O, Andrews M R, van Druten N J, Durfee D S, Kurn D M and Ketterle W 1995a *Phys. Rev. Lett.* **75** 3969

Davis K B, Mewes M O, Joffe M A, Andrews M R and Ketterle W 1995b *Phys. Rev. Lett.* **74** 5202

Dehmelt H 1981 *35th Ann. Frequency Control Symp.* pp 596–601

Deng X L, Porras D and Cirac J I 2005 *Phys. Rev. A* **72** 063407–11

Deng X L, Porras D and Cirac J I 2008 *Phys. Rev. A* **77** 033403–11

Deslauriers L, Olmschenk S, Stick D, Hensinger W K, Sterk J and Monroe C 2006 *Phys. Rev. Lett.* **97** 103007

Diedrich F, Bergquist J C, Itano W M and Wineland D J 1989 *Phys. Rev. Lett.* **62** 403–6

Drewsen M, Brodersen C, Hornekær L, Hangst J S and Schifffer J P 1998 *Phys. Rev. Lett.* **81** 2878

Dubin D H E 1993 *Phys. Rev. Lett.* **71** 2753

Feynman R 1982 *Int. J. Theor. Phys.* **21** 467–88

Feynman R 1986 *Found. Phys.* **16** 507

Fisher M P A, Weichman P B, Grinstein G and Fisher D S 1989 *Phys. Rev. B* **40** 546

Fisher R, Yuan H, Spoerl A and Glaser S 2009 *Phys. Rev. A* **79** 042304

Fishman S, Chiara G D, Calarco T and Morigi G 2008 *Phys. Rev. B* **77** 064111

Frenkel Y and Kontorova T 1938 *Phys. Z. Sowietunion* **13** 1

Friedenauer A, Schmitz H, Glueckert J T, Porras D and Schaetz T 2008 *Nat. Phys.* **4** 757–61

Gaetan A, Miroshnychenko Y, Wilk T, Chotia A, Viteau M, Comparat D, Pillet P, Browaeys A and Grangier P 2009 *Nat. Phys.* **5** 115–8

García-Mata I, Zhirov O V and Shepelyansky D L 2007 *Eur. Phys. J. D* **41** 325–30

Ghosh P K 1995 *Ion Traps* (Oxford: Oxford University Press)

Gibbons G W and Hawking S W 1977 *Phys. Rev. D* **15** 2738–51

Giorgini S, Pitaevskii L P and Stringari S 2008 *Rev. Mod. Phys.* **80** 1215

Girardeau M 1960 *J. Math. Phys., NY* **1** 516–23

Gitterman M and Halpern V 2004 *Phase Transitions: A Brief Account with Modern Applications* (Singapore: World Scientific)

Greiner M, Mandel O, Esslinger T, Hansch T W and Bloch I 2002 *Nature* **415** 39–44

Grotendorst J, Marx D and Muramatsu A 2002 *Quantum Simulations of Complex Many-Body Systems: from Theory to Algorithms* (Jülich: Forschungszentrum)

Hackermuller L, Hornberger K, Brezger B, Zeilinger A and Arndt M 2004 *Nature* **427** 711–4

Häffner H *et al* 2005 *Nature* **438** 643–6

Haljan P C, Brickman K A, Deslauriers L, Lee P J and Monroe C 2005 *Phys. Rev. Lett.* **94** 153602

Hänsch T W and Schawlow A L 1975 *Opt. Commun.* **13** 68

Hebb D O 1949 *The Organization of Behavior* (New York: Wiley)

Heinzen D J and Wineland D J 1990 *Phys. Rev. A* **42** 2977

Heisenberg W 1928 *Z. Phys.* **49** 619–36

Hensinger W K, Olmschenk S, Stick D, Hucul D, Yeo M, Acton M, Deslauriers L, Monroe C and Rabchuk J 2006 *Appl. Phys. Lett.* **88** 034101

Hofstetter W, Cirac J I, Zoller P, Demler E and Lukin M D 2002 *Phys. Rev. Lett.* **89** 220407

Holland M, Kokkelmans S J J M F, Chiofalo M L and Walser R 2001 *Phys. Rev. Lett.* **87** 120406

Home J P and Steane A M 2006 *Quantum Inf. Comput.* **6** 289–325

Hopfield J J 1982 *Proc. Natl Acad. Sci.* **79** 2554–8

Hubbard J 1963 *Proc. R. Soc. A* **276** 238–57

Huber G, Deuschle T, Schnitzler W, Reichle R, Singer K and Schmidt-Kaler F 2008 *New J. Phys.* **10** 013004

Hucul D, Yeo M, Hensinger W K, Rabchuk J, Olmschenk S and Monroe C 2008 *Quantum Inf. Comput.* **8** 0501

Hugh D M and Twamley J 2005 *Phys. Rev. A* **71** 012315

Igloi F, Peschel I and Turban L C 1993 *Adv. Phys.* **42** 683–740

Ising E 1925 *Z. Phys.* **31** 253–8

James D F V 1998 *Appl. Phys.* B **66** 181–90

Jane E, Vidal G, Dür W, Zoller P and Cirac J I 2003 *Quantum Inf. Comput.* **3**

Johanning M, Braun A, Timoney N, Elman V, Neuhauser W and Wunderlich C 2009 *Phys. Rev. Lett.* **102** 073004

Jonathan D and Plenio M B 2001 *Phys. Rev. Lett.* **87** 127901

Jonathan D, Plenio M B and Knight P L 2000 *Phys. Rev. A* **62** 042307

Kielpinski D, Monroe C and Wineland D J 2002 *Nature* **417** 709–11

Kjærgaard N and Drewsen M 2003 *Phys. Rev. Lett.* **91** 095002

Klein O 1929 *Z. Phys. A* **53** 157–65

Labaziewicz J, Ge Y, Antohi P, Leibrandt D, Brown K R and Chuang I L 2008 *Phys. Rev. Lett.* **100** 013001

Lamata L, Leon J, Schatz T and Solano E 2007 *Phys. Rev. Lett.* **98** 253005

Leggett A J, Chakravarty S, Dorsey A T, Fisher M P A, Garg A and Zwerger W 1987 *Rev. Mod. Phys.* **59** 1

Leibfried D, Meekhof D M, King B E, Monroe C, Itano W M and Wineland D J 1996 *Phys. Rev. Lett.* **77** 4281–5

Leibfried D, Meekhof D M, Monroe C, King B E, Itano W M and Wineland D J 1997 *J. Mod. Opt.* **44** 2485–505

Leibfried D *et al* 2002 *Phys. Rev. Lett.* **89** 247901

Leibfried D *et al* 2003 *Nature* **422** 412–5

Leibfried D *et al* 2005 *Nature* **438** 639–42

Lenz W 1920 *Phys. Z.* **21** 613

Lieb E H and Liniger W 1963 *Phys. Rev.* **130** 1605

Loewen M and Wunderlich C 2004 *Verhandl. DPG* **VI 39** 7/113

Lougovski P, Walther H and Solano E 2006 *Eur. Phys. J. D* **38** 423–6

Luttinger J M 1963 *J. Math. Phys., NY* **4** 1154

Meekhof D M, Monroe C, King B E, Itano W M and Wineland D J 1996a *Phys. Rev. Lett.* **76** 1796

Meekhof D M, Monroe C, King B E, Itano W M and Wineland D J 1996b *Phys. Rev. Lett.* **77** 2346

Menicucci N C and Milburn G J 2007 *Phys. Rev. A* **76** 052105–5

Metcalf H J and van der Straten P 2001 *Laser Cooling and Trapping* (Berlin: Springer)

Meyrath T P, Schreck F, Hanssen J L, Chuu C S and Raizen M G 2005 *Phys. Rev.* A **71** 041604

Mezard M, Parisi G and Virasoro M A 1987 *Spin Glass Theory and Beyond* (Singapore: World Scientific)

Milburn G J 1999 arXiv:quant-ph/9908037

Milburn G J, Schneider S and James D F V 2000 *Fortschr. Phys.* **48** 801–10

Mintert F and Wunderlich C 2001 *Phys. Rev. Lett.* **87** 257904

Mintert F and Wunderlich C 2003 *Phys. Rev. Lett.* **91** 029902

Mitchell T B, Bollinger J J, Dubin D H E, Huang X P, Itano W M and Baughman R H 1998 *Science* **282** 1290–3

Molmer K and Sorensen A 1999 *Phys. Rev. Lett.* **82** 1835–8

Monroe C, Meekhof D M, King B E, Itano W M and Wineland D J 1995a *Phys. Rev. Lett.* **75** 4714

Monroe C, Meekhof D M, King B E, Jefferts S R, Itano W M, Wineland D J and Gould P 1995b *Phys. Rev. Lett.* **75** 4011–4

Monroe C, Meekhof D M, King B E and Wineland D J 1996a *Science* **272** 1131–6

Monroe C R, Meekhof D M, Leibfried D, King B E, Itano W M and Wineland D J 1996b *Opt. Photon. News* **7** 13–4

Morigi G and Fishman S 2004a *Phys. Rev. Lett.* **93** 170602

Morigi G and Fishman S 2004b *Phys. Rev.* E **70** 066141

Morsch O and Oberthaler M 2006 *Rev. Mod. Phys.* **78** 179

Müller M, Liang L, Lesanovsky I and Zoller P 2008 *New J. Phys.* **10** 093009

Neuhauser W, Hohenstatt M, Toschek P E and Dehmelt H 1980 *Phys. Rev.* A **22** 1137

Nightingale M P and Umrigar C J 1998 *Quantum Monte Carlo Methods in Physics and Chemistry* (Berlin: Springer)

Onsager L 1944 *Phys. Rev.* **65** 117

Ospelkaus C, Langer C E, Amini J M, Brown K R, Leibfried D and Wineland D J 2008 *Phys. Rev. Lett.* **101** 090502

Osterloh A, Amico L, Falci G and Fazio R 2002 *Nature* **416** 608–10

Paredes B, Widera A, Murg V, Mandel O, Fölling S, Cirac I, Shlyapnikov G V, Hänsch T W and Bloch I 2004 *Nature* **429** 277–81

Peitgen H O, Jürgens H and Saupe D 2004 *Chaos and Fractals: New Frontiers of Science* 2nd edn (New York: Springer)

Pfeuty P 1970 *Ann. Phys.* **57** 79–90

Platini T, Karevski D and Turban L 2007 *J. Phys. A: Math. Theor.* **40** 1467–79

Plenio M and Huelga S 2008 *New J. Phys.* **10** 113019

Plenio M B and Virmani S 2007 *Quantum Inf. Comput.* **7** 1

Pons M, Ahufinger V, Wunderlich C, Sanpera A, Braungardt S, Sen A, Sen U and Lewenstein M 2007 *Phys. Rev. Lett.* **98** 023003

Porras D and Cirac J I 2004a *Phys. Rev. Lett.* **92** 207901

Porras D and Cirac J I 2004b *Phys. Rev. Lett.* **93** 263602

Porras D, Marquardt F, Delft J v and Cirac J I 2008 *Phys. Rev.* A **78** 010101

Powell H F, Segal D M and Thompson R C 2002 *Phys. Rev. Lett.* **89** 093003

Raizen M G, Gilligan J M, Bergquist J C, Itano W M and Wineland D J 1992 *Phys. Rev.* A **45** 6493

Reichle R, Leibfried D, Blakestad R B, Britton J, Jost J D, Knill E, Langer C, Ozeri R, Seidelin S and Wineland D J 2006 *Fortschr. Phys.* **54** 666–85

Retzker A, Thompson R C, Segal D M and Plenio M B 2008 *Phys. Rev. Lett.* **101** 260504

Riebe M *et al* 2004 *Nature* **429** 734–7

Rojas R 1996 *Neural Networks—A Systematic Introduction* (Berlin: Springer)

Rosenband T *et al* 2008 *Science* **319** 1808–12

Rowe M A *et al* 2002 *Quantum Inf. Comput.* **2** 257–71

Sachdev S 1999 *Quantum Phase Transitions* (Cambridge: Cambridge University Press)

Sackett C A *et al* 2000 *Nature* **404** 256–9

Santos M F, Giedke G and Solano E 2007 *Phys. Rev. Lett.* **98** 020401

Sasura M and Steane A M 2003 *Phys. Rev.* A **67** 19

Schiffer J P 1993 *Phys. Rev. Lett.* **70** 818

Schmidt-Kaler F, Häffner H, Riebe M, Gulde S, Lancaster G P T, Deuschle T, Becher C, Roos C F, Eschner J and Blatt R 2003 *Nature* **422** 408–11

Schmied R, Roscilde T, Murg V, Porras D and Cirac J I 2008 *New J. Phys.* **10** 045017

Schollwöck U, Richter J, Farnell D and Bishop R 2004 *Quantum Magnetism* (*Lecture Notes in Physics* vol 645) (Berlin: Springer)

Schrödinger E 1935 *Naturwissenschaften* **23** 807–12

Schulte T *et al* 2006 *Acta Phys. Pol.* A **109** 89–99

Schulz S, Poschinger U, Singer K and Schmidt-Kaler F 2006 *Fortschr. Phys.* **54** 648–65

Schützhold R, Uhlmann M, Petersen L, Schmitz H, Friedenauer A and Schätz T 2007 *Phys. Rev. Lett.* **99** 201301–4

Schwabl F 1997 *Quantenmechanik für Fortgeschrittene* (Berlin: Springer)

Seidelin S *et al* 2006 *Phys. Rev. Lett.* **96** 253003–4

Sørensen A and Mølmer K 2000 *Phys. Rev.* A **62** 022311

Stahl S, Galve F, Alonso J, Djekic S, Quint W, Valenzuela T, Verdú J, Vogel M and Werth G 2005 *Eur. Phys. J.* D **32** 139

Steane A 1997 *Appl. Phys.* B **64** 623–43

Stenholm S 1986 *Rev. Mod. Phys.* **58** 699

Stick D, Hensinger W K, Olmschenk S, Madsen M J, Schwab K and Monroe C 2006 *Nat. Phys.* **2** 36–9

Thaller B 1992 *The Dirac Equation Texts and Monographs in Physics* (Berlin: Springer)

Tolra B L, O'Hara K M, Huckans J H, Phillips W D, Rolston S L and Porto J V 2004 *Phys. Rev. Lett.* **92** 190401

Turchette Q A *et al* 2000 *Phys. Rev.* A **61** 8

Unruh W G 1976 *Phys. Rev.* D **14** 870–92

Urban E, Johnson T A, Henage T, Isenhower L, Yavuz D D, Walker T G and Saffman M 2009 *Nat. Phys.* **5** 110–4

Voit J 1995 *Rep. Prog. Phys.* **58** 977

Waki I, Kassner S, Birkl G and Walther H 1992 *Phys. Rev. Lett.* **68** 2007

Wallentowitz S, Vogel W, Siemers I and Toschek P E 1996 *Phys. Rev.* A **54** 943

Wang S X, Labaziewicz J, Ge Y, Shewmon R and Chuang I L 2008 arXiv:0811.2422v1

Weiss U 1999 *Quantum Dissipative Systems* (Singapore: World Scientific)

White S R 1993 *Phys. Rev.* B **48** 10345

Wineland D J and Dehmelt H 1975 *Bull. Am. Phys. Soc.* **20** 637

Wineland D J and Itano W M 1979 *Phys. Rev.* A **20** 1521–40

Wineland D J, Monroe C, Itano W M, King B E, Leibfried D, Myatt C and Wood C 1998 *Phys. Scr.* T **76** 147

Wineland D J, Monroe C, Itano W M, Leibfried D, King B E and Meekhof D M 1998 *J. Res. Natl Inst. Stand. Technol.* **103** 259–328

Wunderlich C 2002 *Laser Physics at the Limit* ed H Figger, D Meschede and C Zimmermann (Berlin: Springer) pp 261–71

Wunderlich C and Balzer C 2003 *Advances in Atomic Molecular, and Optical Physics* vol 49 (San Diego, CA: Academic) pp 293–372

Wunderlich C, Morigi G and Reiß D 2005 *Phys. Rev.* A **72** 023421

Wunderlich H, Wunderlich C, Singer K and Schmidt-Kaler 2009 *Phys. Rev.* A **79** 052324

Zhirov O V, Casati G and Shepelyansky D L 2002 *Phys. Rev.* E **65** 026220